



UNIVERSITY OF DORTMUND



DELTA: INT. REP. 001-05

# Synchrotron radiation sources at DELTA\*

D. Schirmer

University of Dortmund,  
Institute of Acceleratorphysics and Synchrotronradiation  
email: [schirmer@delta.uni-dortmund.de](mailto:schirmer@delta.uni-dortmund.de)

January 2005

## Abstract

This report summarizes the main machine parameters and synchrotron radiation properties of different synchrotron radiation sources at DELTA (Status 1/2005).

\*Non-complete draft version!

Dr. Detlev Schirmer  
University of Dortmund  
Center of Synchrotron Radiation (ZfSy)  
Maria-Goeppert-Mayer Str. 2  
44221 Dortmund  
email: [schirmer@delta.uni-dortmund.de](mailto:schirmer@delta.uni-dortmund.de)

# Contents

<b>1</b>	<b>Introduction</b>	<b>1</b>
<b>2</b>	<b>Calculation of the synchrotron radiation properties</b>	<b>7</b>
2.1	Synchrotron radiation intensities . . . . .	7
2.2	Brightness and source emittance . . . . .	13
2.3	Pulsed time structure . . . . .	17
<b>3</b>	<b>Dipole Radiation</b>	<b>19</b>
<b>4</b>	<b>SAW Radiation</b>	<b>27</b>
<b>5</b>	<b>Undulator Radiation</b>	<b>39</b>
5.1	U-250 . . . . .	39
5.2	U-55 . . . . .	44
<b>A</b>	<b>Definitions</b>	<b>51</b>
<b>B</b>	<b>A numerical approximation of the Bessel Function</b>	<b>53</b>
B.1	Natural opening angle of the synchrotron radiation . . . . .	55
<b>C</b>	<b>Comparison to other Synchrotron Radiation Sources</b>	<b>57</b>
	<b>List of Figures</b>	<b>63</b>
	<b>List of Tables</b>	<b>65</b>
	<b>Bibliography</b>	<b>67</b>



# 1 Introduction

DELTA (**D**ortmunder **E**lectron **A**ccelerator) is a 1.5 GeV synchrotron light source located at the University of Dortmund in Germany. The facility, dedicated for accelerator physics as well as for synchrotron radiation (SR) based experiments, is in routine operation since summer 1998 [1],[2],[3],[4]. Start of user operation took place in March 1999 by the Forschungszentrum Jülich (BL-5). Figure 1.1 shows the magnet lattice and dedicated beam lines (BL0 - BL12) of the facility DELTA, including the 75 MeV s-band **l**inear **a**ccelerator (Linac), the 1.5 GeV full energy booster synchrotron BoDo (**B**ooster **D**ortmund) and the main electron storage ring (Delta) with a circumference of 115.2 m. The main purpose of DELTA is the generation of synchrotron radiation. This electromagnetic radiation is created by the transverse acceleration of high energy charged particles (e.g. electrons or positrons) either in bending magnets or in dedicated insertion devices (e.g. wiggler (SAW) or undulator magnets (U55, U250)) assembled in the straight section of the storage ring.

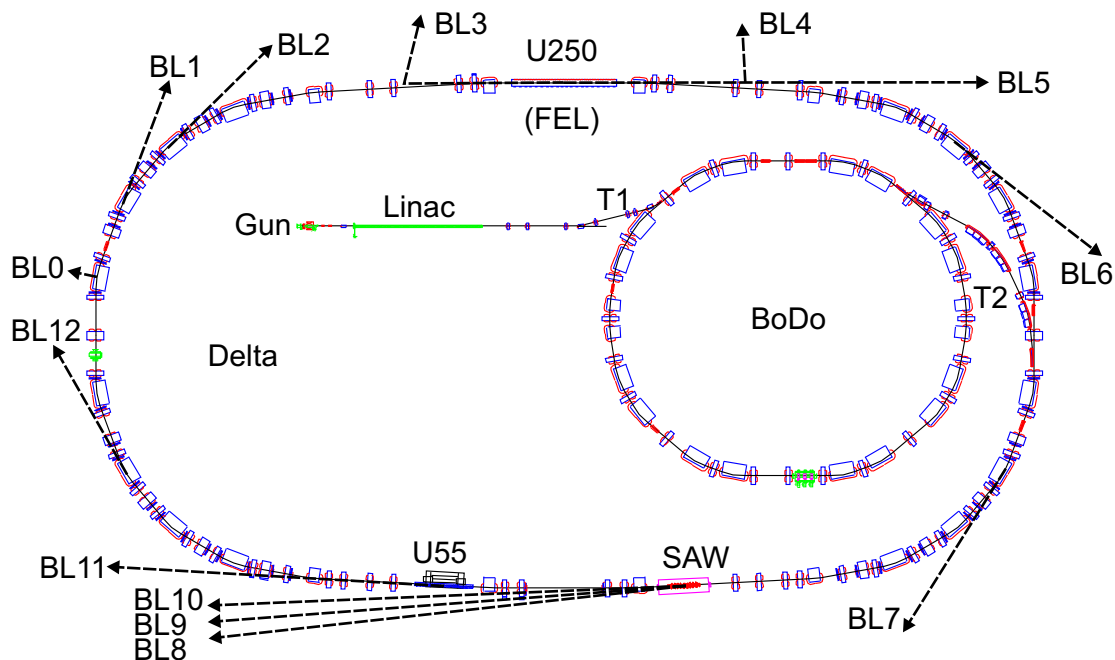


Fig. 1.1: Beamlines and magnet lattice of the DELTA facility.

In consideration of all planned SR experiments the following magnet types can be used as SR sources:

- DELTA lattice dipoles (BL-0 (infra-red (IR)), BL-1,2,6,7,12)
- Superconducting asymmetric multipole wiggler (SAW) (BL-8,9,10)
  - symmetrical mode
  - asymmetrical mode with variable degree of circular polarization rate
  - undulator mode
- Undulators:
  - U250: electromagnetic Free Electron Laser (FEL) undulator (BL-5, BL-3,4 FEL-Mode)
  - U55: permanent magnet hybrid undulator (BL-11)

Table 1.1 summarizes the main machine parameters and operating data.

DELTA serves universities and industries as a source of synchrotron radiation on a regional level. The facility is operated for 3000 hours per year and the average availability of the accelerators remained nearly constant at a level of approximately 90 %.

Up to now, DELTA provides seven beamlines. In addition to three hard X-ray SAW beamlines (BL-8,9,10), two undulator beamlines for photon energies between 5 and 400 eV (BL-5, U250) and between 55 and 1500 eV (BL-11, U55) as well as two bending magnet beamlines up to 200 eV are in operation or in the commissioning phase. The brilliance, flux density and photon flux of the various DELTA synchrotron radiation sources are summarized in the figures 1.2, 1.3 and 1.4. Further details are discussed in the corresponding chapters 3, 4 and 5.

The SAW center beamline (BL-9) of DELTA is fully operational since January 2002. The radiation supplied by the SAW, which has a critical photon energy of 7.9 keV, is monochromatised by a Si 311 double crystal monochromator. The second sagittal focusing monochromator crystal allows for a horizontal beam size less than 2 mm at the sample position. The monochromator covers an energy range from 5 keV up to 30 keV with a photon flux of about  $3 \times 10^{10}$  photons/s/mm<sup>2</sup> at 9 keV (electron beam current: 120 mA). A complete program with numerous external users from different places has been established at this beamline.

Two experimental endstations are installed permanently, a Huber 6-circle diffractometer and a Rowland type single crystal fluorescence spectrometer. Furthermore, a microfocus energy dispersive x-ray fluorescence (EDXRF) setup is accessible and an XMCD (x-ray magnetic circular dichroism) setup can be used for students practices. In addition a scattering chamber equipped with a Si 800 analyser crystal for x-ray Raman and inelastic x-ray scattering measurements with 1.2 eV resolution is available [5],[6],[7].

The University of Wuppertal/Siegen (Germany) took over the responsibility for the remaining SAW beamlines BL-10 and BL-8. The latter has been ordered by the company ACCEL

(Bergisch Gladbach, Germany)[8]. Since autumn 2006 the beamline BL-8 is fully operational. BL-10 is under construction.

The Dortmund undulator (U55) beamline BL-11 was delivered and mounted during the summer shutdown 2003 by the company FMB (Berlin, Germany). This beamline is fully operational since autumn 2006 and provides synchrotron radiation in the energy range between 55 and 1500 eV. The beamline uses a PGM-setup with two gratings (400 and 1200 lines/mm) and a variable exit slit up to 3 mm. The planned experiments are photoemission spectroscopy (XPS) and photoelectron diffraction pattern (XPD) of the interface layer of semiconductors [6],[7].

The Forschungszentrum Jülich (Germany) will continue the utilization of the undulator U250 and operation of BL-5.

First synchrotron light was seen at the bending magnet beamline BL-12, the former TGM3 of BESSY-I, now operated by the group Experimental Physics Ib at the department of Physics of the University of Dortmund. The TGM3-Beamline is still under commissioning and will provide radiation in the range between 6 and 200eV [9].

The Institute for Analytical Sciences (ISAS) in Dortmund, took over the responsibility and support for the soft X-ray dipole beamline BL-2 and the infra-red beamline BL-0. Since 2004 BL-2 is used for a excitation source for X-ray fluorescence spectrometry (XRF). Additionally, a precise goniometer will be installed for X-ray standing waves (XSW) measurements. ISAS is working mainly in the field of the development of analytical tools for industrial applications. It is planned to install a scientific program in the field of applied spectroscopy [7],[6].

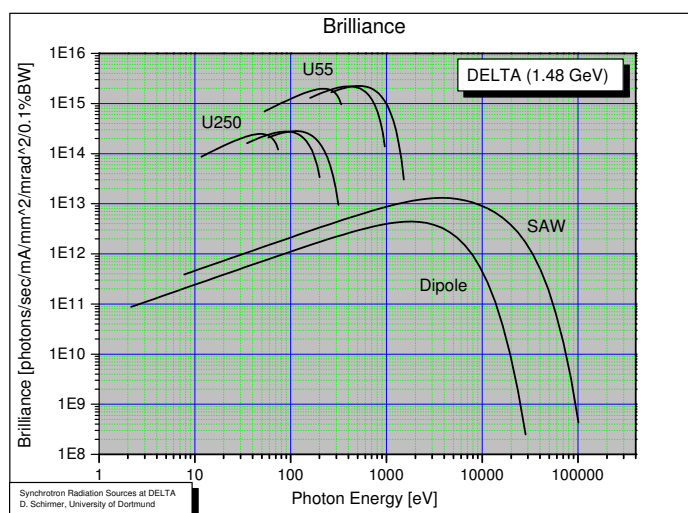


**Fig. 1.2:** Brilliance of various SR-sources at DELTA (electron beam current: 1 mA, horizontal emittance: 16 nm rad at 1.48 GeV).

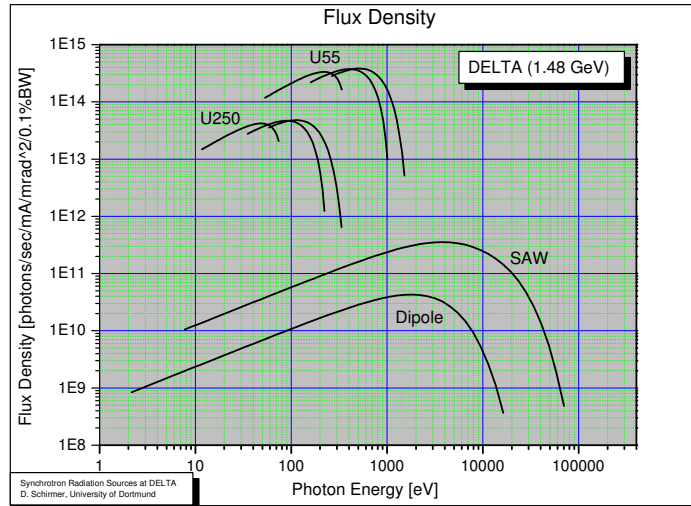


**Fig. 1.3:** Photon flux density of various SR-sources at DELTA (electron beam current: 1 mA, horizontal emittance: 16 nm rad at 1.48 GeV).

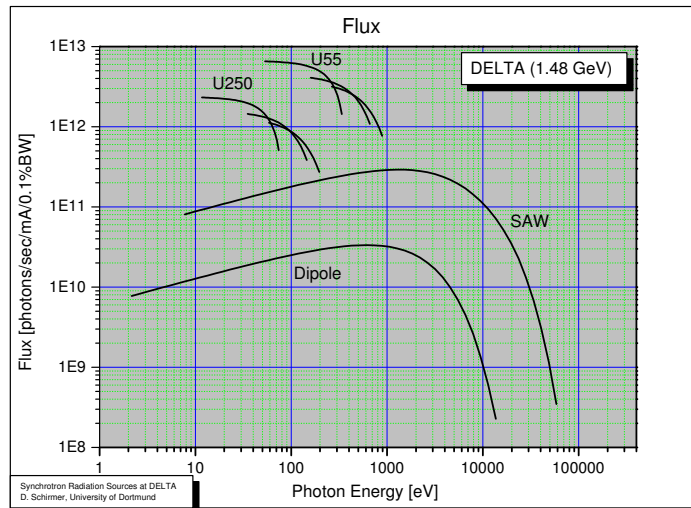


**Fig. 1.4:** Photon flux of various SR-sources at DELTA (electron beam current: 1 mA, horizontal emittance: 16 nm rad at 1.48 GeV).

Energy	max. 1.5 GeV	450 MeV - 1.5 GeV
Length Storage Ring	115.2 m	
Insertion Devices	3	Superconducting Asymmetric Multipole Wiggler, $B_{max} = 5.3$ T, $E_c = 7.9$ keV @ 1.5 GeV)/ Hybrid-PM-Undulator U55/ Electromagn. Undulator U250
Start of User Operation	3/1999	FZ Jülich Beamline (BL-5)
Number of Beamlines	12	not all fully equipped
Number of Bending Magnet Beamlines	5	BL-0,2,12 in user operation BL-6,7 for accelerator diagnostics
Number of Undulator Beamlines	2	@ the U250, in operation (BL-5) @ the U55, in operation (BL-11)
Number of Wiggler Beamlines	3	1 in construction (BL-10)/ 2 in operation (BL-9,8)
Number of Beamlines at the FEL	2	also for storage ring diagnostics
Annual Scheduled User Beamtime	approx. 2000 h	3000 h total machine operation
Horiz. Electron Beam Emittance	15 nm rad	nominal @ 1.5 GeV
Vert. Electron Beam Emittance	1.5 nm rad	nominal @ 1.5 GeV
Energy spread $\Delta E/E$	$7 \cdot 10^{-7}$	nominal @ 1.5 GeV
Bunch Length	36 ps	@ standard multibunch mode
Effective Beam Size at U250	horiz./vertical 160 $\mu m$ /140 $\mu m$	@ 1.5 GeV/future reduction by a factor of 2 horizontally
Effective Beam Size at U55	360 $\mu m$ /80 $\mu m$	@ 1.5 GeV/dito
Effective Beam Size at Wiggler	360 $\mu m$ /80 $\mu m$	@ 1.5 GeV/dito
RF-Frequency	500 MHz	
Beam Current	150 mA	max. current @ 1.5 GeV and standard multi bunch mode
Beam Lifetime (1/e)	20 mA 10 h	in single bunch mode @ 1.5 GeV/100 mA data taken in 2003
Filling time	20 min 10 - 15 min	@ 1 GeV / 20 mA single bunch @ 1.5 GeV / 120 mA multi bunch

**Tab. 1.1:** *Important machine and operating parameters (Status 1/2005).*



## 2 Calculation of the synchrotron radiation properties

### 2.1 Synchrotron radiation intensities

The synchrotron radiation, being emitted tangential to the orbit of the electron beam, has several outstanding properties. The most important features are:

- High intensity (extremely bright)
- Broad spectral range (from UV up to X-ray)
- High degree of polarization
- Natural collimation with a very small opening angle
- Precise pulsed time structure
- Extreme small source spot size

These qualities make it an important experimental tool for a wide range of scientific and technological applications. It is perfectly suited to investigate the structure and properties of matter. Applications include solid state physics, chemistry, biology, medicine and lithography for microstructure technology. The characteristics of the synchrotron radiation has been derived and described in detail in several reports leading back to G.A. Schott (1912)[10].

The basic equation describing the radiation of an relativistic charged particle have been given by Schwinger [11], Sokolov/Ternov [12] and Jackson [13]:

$$\frac{d^2 F}{d\Omega d\omega} = \frac{\alpha\omega^2}{4\pi^2} \left| \int_{-\infty}^{+\infty} [\vec{n} \times (\vec{n} \times \vec{\beta})] \cdot e^{i\omega(t - \vec{n} \cdot \vec{r}(t)/c)} dt \right|^2 \quad (2.1)$$

This relation describes the spectral distribution of intensity per solid angle  $d\Omega$  of an ideal (i.e. punctual and monoenergetic) electron (or positron) beam along the trajectory  $\vec{r}(t)$ . With  $\alpha \hat{=} \text{fine structure constant}$ ,  $\vec{n}(t) \hat{=} \text{the unit vector in direction of emission}$  and  $\vec{\beta}(t) = \frac{\vec{v}}{c}$  with  $\vec{v}(t) \hat{=} \text{velocity of the particle}$ . Whereby an outer field of force (magnetic or electric) defines the motion of the particle and consequently the radiation properties. Figure 2.1 illustrates the coordinate system used. In the calculations the black box represents any desired radiation source (dipole, wiggler, undulator, solenoid, ...) with an arbitrary magnetic

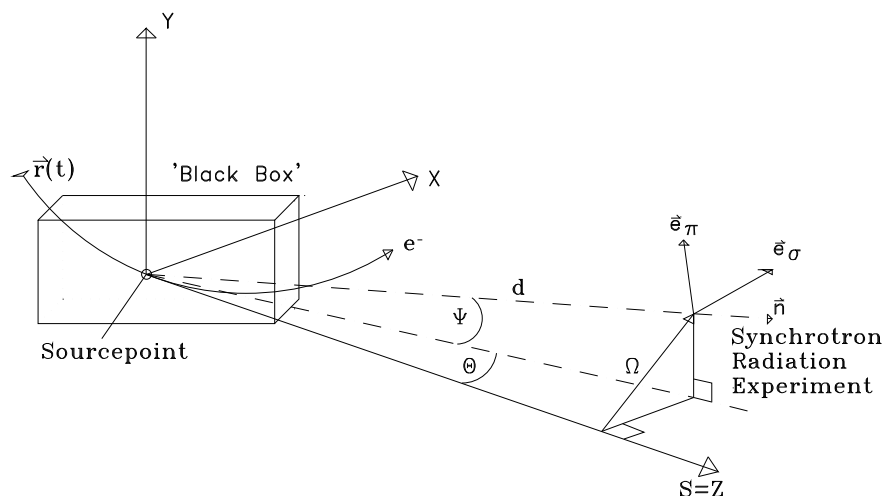


**Fig. 2.1:** Coordinate system to describe the motion of charged particles and the angular dependence of the synchrotron radiation properties.

field distribution<sup>1</sup>. Thus the motion of a charged particle depends mainly on the field distribution whereby the dynamics (equation of motion) is given by the relativistic Lorentz force:

$$\vec{F}_L = \dot{\vec{p}} = \frac{d}{dt}(\gamma m_e \vec{v}) = e \cdot \vec{v} \times \vec{B} \quad (2.2)$$

with

$$\gamma = \frac{E_e}{m_e c^2} = \left[ 1 - \frac{v^2}{c^2} \right]^{-1/2} \gg 1. \quad (2.3)$$

The black box can be divided into in the following categories:

I. The magnetic field is given by an analytical function/expression:

(1.)  $B_y(s) = (\text{piecewise}) \text{ constant} \implies$  dipole or 'wavelength-shifter'

(2.)  $B_y(s) \sim B_{y0} \sin(2\pi s/\lambda_w)$  alternatively  $\sim B_{y0} \cos(2\pi s/\lambda_w)$   
 $\implies$  planar, symmetrical and periodical field with  $K = \frac{e}{2\pi m_e c} \cdot \lambda_w B_{y0}$ :

(a)  $K \ll 1 \implies$  weak field undulator  $\implies$  only 1. harmonic important

(b)  $K \geq 1 \implies$  strong field undulator  $\implies$  n discrete harmonics

(c)  $K \gg 1 \implies$  wiggler limit  $n \rightarrow \infty \implies$  continuum

(3.)  $B_y(s) \sim B_{y1} \sin(4\pi s/\lambda_w) + B_{y2} \cos(2\pi s/\lambda_w)$  und  $K \gg 1$   
 $\implies$  asymmetrical but planar and periodical field in the so called wiggler limit

<sup>1</sup>Electric fields are negligible because at relativistic velocities, electric fields and magnetic fields have the same effect if  $E = cB$ .

- (4.)  $B(s) \sim B_{x_0} \sin(2\pi s/\lambda_w) + B_{y_0} \cos(2\pi s/\lambda_w)$   
 $\implies$  periodical but not planar structure with  $K_{x,y} = 93.4 \cdot \lambda_w [m] \cdot B_{x_0,y_0} [T]$
- (a)  $K_x = K_y \implies$  helical (crossed overlapped) wiggler/undulator
- (b)  $K_x \neq K_y \implies$  elliptical wiggler/undulator
- (c)  $K_x = 0$  or  $K_y = 0 \implies$  planar vertical or horizontal wiggler/undulator

II. The field distribution must be solved by numerical methods or is represented by measured data if the progression of the magnetic field is more or less arbitrary and determined by the complex geometry of the insertion device. Mostly the field can be divided into the above listed types of magnets (see chapter 4 and 5).

In the most frequent case, with piecewise and constant magnetic fields (dipole, strong wiggler, wavelength shifter) i.e. circular trajectories within the midplane, one can summarize the calculation of J. Schwinger by the following basic formular:

$$\frac{d^2 F_D(\omega)}{d\theta d\psi} = \frac{3\alpha}{4\pi^2} \gamma^2 \frac{\Delta\omega}{\omega} \frac{I}{e} F_s(\xi, \gamma\psi) \quad (2.4)$$

with

$$F_s(\xi, \gamma\psi) = F_s^\sigma + F_s^\pi = y^2(1 + X^2)^2 \cdot \left[ K_{2/3}^2(\xi) + \frac{X^2}{1 + X^2} K_{1/3}^2(\xi) \right] \quad (2.5)$$

With  $X = \gamma\psi$ ,  $\xi = \frac{y}{2}(1 + X^2)^{3/2}$  and using the abbreviations and substitutions listed in table 2.1 one can calculate all essential radiation characteristics as:

- Spectral and angular distribution of the radiated power and photon flux.
- Rate of polarization (linear/circular) in dependence of emission angle and photon energy.
- Any combinations of emission angle and/or photon energy integrated spectra.

To compute the above mentioned SR properties, it is reasonable to separate the photon flux in a portion of parallel  $F_s^\sigma$  and perpendicular  $F_s^\pi$  rate in reference to the accelerator plane. For a vanishing evaluation angle  $\psi = 0$  (i.e. in the midplane) the second term in equation 2.5 cancels down and the radiation is absolutely linear polarized. Due to the fact, that the components of the rotating electrical field vector have a constant phase difference of  $\pi/2$ , one gets elliptical polarization above and below the midplane ( $\psi \neq 0$ ). This elliptical polarization can be separated in a horizontal and a vertical part. The ratio of the small  $a$  and the large  $b$  principal axis of the polarization ellipse is then given by

$$r = \frac{a}{b} = \frac{\gamma\psi K_{1/3}(\xi)}{\sqrt{1 + (\gamma\psi)^2} K_{2/3}(\xi)} \quad (2.6)$$

For  $\gamma\psi \gg 1$  the ratio  $r \rightarrow 1$  and one gets completely circular polarization, whereas the intensity runs off due to  $F_s \rightarrow 0$ . Furthermore, the rotating direction (helicity) of the electrical field vector switches when changing the sign of the vertical viewing angle  $\psi$  or the polarity of the magnetic field  $B$ .

Due to the fact, that the radiation is high-grade collimated in the vertical direction ("Lorentz-boost":  $\sim 1/\gamma$ ), it is common to specify the vertical integrated intensity. The integration of equation 2.4 over the vertical angle  $\psi$  results in (e.g. [14]):

$$\frac{dF_D(\omega)}{d\theta} = \frac{\alpha\gamma\sqrt{3}}{4\pi} \frac{\Delta\omega}{\omega} \frac{I}{e} y F_s(y) \quad (2.7)$$

with

$$F_s(y) = F_s^\sigma + F_s^\pi = \int_y^\infty K_{5/3}(y') dy' + K_{2/3}(y) + \int_y^\infty K_{5/3}(y') dy' - K_{2/3}(y) \quad (2.8)$$

Addition of both polarization components yield in:

$$\frac{dF_D(\omega)}{d\theta} = \frac{\alpha\gamma\sqrt{3}}{2\pi} \frac{\Delta\omega}{\omega} \frac{I}{e} y \int_y^\infty K_{5/3}(y') dy' \quad (2.9)$$

For the intensity in the forward direction (on axis) one gets with equation 2.4 and  $\psi = 0$ :

$$\left. \frac{d^2 F_D(\omega)}{d\theta d\psi} \right|_{\psi=0} = \frac{3\alpha}{4\pi^2} \gamma^2 \frac{\Delta\omega}{\omega} \frac{I}{e} y^2 K_{2/3}^2(y/2) \quad (2.10)$$

The collimation depends strongly on the photon wavelength. Under the assumption of a gaussian vertical angle distribution with a half rms-divergence  $\sigma_\psi$  and the equations 2.9 and 2.10 one can estimate the collimation in good approximation to:

$$\sigma_\psi \sqrt{2\pi} = \frac{\frac{dF_D}{d\theta}}{\left. \frac{d^2 F_D}{d\theta d\psi} \right|_{\psi=0}} = \sqrt{\frac{2\pi}{3}} (\gamma y)^{-1} \frac{\int_y^\infty K_{5/3}(y') dy'}{K_{2/3}^2(y/2)} \equiv \frac{1}{\gamma} \cdot C(y) \quad (2.11)$$

Multiplying equation 2.4 with  $\hbar\omega$  one gets the spectral power per solid angle element  $d\Omega$ . By exchanging  $\Delta\omega$  into  $d\omega$  in equation 2.4 one obtains the corresponding angular distribution of the radiated power for the total electron beam current  $I$ . Finally resulting in

$$\frac{d^2 P}{d^2 \Omega} = \left. \frac{d^2 P}{d^2 \Omega} \right|_{\psi=0} \cdot P_s(X) \quad (2.12)$$

with

$$P_s(X) = \overbrace{(1 + X^2)^{-5/2}}^{P_s^\sigma} + \overbrace{(1 + X^2)^{-5/2} \frac{5}{7} \frac{X^2}{1 + X^2}}^{P_s^\pi} \quad (2.13)$$

and the power density in the forward direction

$$\left. \frac{d^2 P}{d^2 \Omega} \right|_{\psi=0} = \frac{7}{16\pi} \alpha \hbar c \frac{\gamma^5 I}{R e}. \quad (2.14)$$

Whereas  $R$  denotes the bending radius of the electron trajectory. Furthermore, integrating equation 2.12 over all vertical angles gives the total radiated power for both polarization components

$$P_{tot} = P^\sigma + P^\pi = \frac{2}{3} \frac{I \gamma^4}{e R} \alpha \hbar c \Delta\theta \cdot \left( \overbrace{\frac{7}{8}}^{P^\sigma} + \overbrace{\frac{1}{8}}^{P^\pi} \right) \quad (2.15)$$

Finally, one gets the well known  $E^4$ -dependence for the total SR-power per azimuthal angle  $\Delta\theta \cong \frac{\Delta L}{R}$  (here  $\Delta L$  is the length of the electron trajectory arc). In practical units:

$$\frac{P_{tot}}{\Delta\theta} \left[ \frac{mW}{mrad} \right] = 1.27 \cdot E^2[GeV] \cdot B^2[T] \cdot R[m] \cdot I[MA] = 14.08 \cdot \frac{E^4[GeV] \cdot I[MA]}{R[m]} \quad (2.16)$$

The energy loss per turn  $U_0$  calculates by:

$$U_0 = \frac{P_{tot} 2\pi}{I} \hat{=} U_0[KeV] = \frac{88.47 E^4[GeV]}{R[m]} \quad (2.17)$$

Integrating equation 2.9 not over all frequencies but only up to  $y = 1$ , i.e.  $\omega = \omega_c$ , it appears, that the spectrum of the synchrotron radiation is divided into two identical fractions of power. This is the definition of the critical (typical) photon energy.

As can be seen in equation 2.6, the polarization depends on the wavelength and the emission angle. By using equation 2.15 and integrating over all angles and frequencies one can deduce another important property of the polarization. With

$$\tau_{lin} = \frac{P_s^\sigma - P_s^\pi}{P_s^\sigma + P_s^\pi} \quad \text{and} \quad \tau_{circ} = \sqrt{1 - \tau_{lin}^2} \quad (2.18)$$

follows, that the maximum amount of linear and circular polarization is  $\tau_{lin} = 75\%$  and  $\tau_{circ} = 66\%$  respectively.

$F_D$	[photons/sec]	$\hat{=}$ photon flux (or intensity $I$ )
$\theta$	[rad]	$\hat{=}$ horizontal emission angle
$\psi$	[rad]	$\hat{=}$ vertical emission angle
$\Omega$	[sr]	$\hat{=}$ solid angle
$I$	[A]	$\hat{=}$ electron beam current
$E_e$	[eV]	$\hat{=}$ electron beam energy
$B$	[T]	$\hat{=}$ magnetic field strength
$R$	[m]	$\hat{=}$ bending radius of electron trajectory: $3.3356 \cdot E_e[\text{GeV}]/B[\text{T}]$
$\alpha$	--	$\hat{=}$ fine structure constant: $e^2/(4\pi\epsilon_0\hbar c) = 1/137.04$
$\gamma$	--	$\hat{=}$ Lorentz factor: $E_e/(m_e c^2)$
$m_e$	[eV/c <sup>2</sup> ]	$\hat{=}$ electron mass: $0.511 [\text{MeV}/c^2]$
$r_e$	[m]	$\hat{=}$ classical electron radius: $2.8179 \cdot 10^{-15} [\text{m}]$
$Z_0$	[ $\Omega$ ]	$\hat{=}$ vacuum impedance: $376.73 [\Omega]$
$c$	[m/s]	$\hat{=}$ speed of light: $2.998 \cdot 10^8 [\text{m}/\text{s}]$
$e$	[C]	$\hat{=}$ electron charge magnitude: $1.6022 \cdot 10^{-19} [\text{C}]$
$\hbar = \frac{h}{2\pi}$	[eV · s]	$\hat{=}$ Planck's constant: $6.582 \cdot 10^{-16} [\text{eV} \cdot \text{s}]$
$\omega$	[Hz]	$\hat{=}$ frequency of the photon
$\epsilon = \hbar\omega$	[eV]	$\hat{=}$ energy of the photon
$\epsilon_c$	[eV]	$\hat{=}$ critical photon energy: $\frac{3\hbar c\gamma^3}{2R}$ $\hat{=}$ $\epsilon_c[\text{KeV}] = 0.6651 B[\text{T}] E_e^2[\text{GeV}^2]$
$\lambda_c$	[m]	$\hat{=}$ critical photon wavelength: $\frac{4\pi R}{3\gamma^3}$ $\hat{=}$ $\lambda_c[\text{\AA}] = 18.64 B^{-1}[\text{T}^{-1}] E_e^{-2}[\text{GeV}^{-2}]$
$\omega_c$	[Hz]	$\hat{=}$ critical photon frequency: $\frac{3\gamma^3 c}{2R}$ $\hat{=}$ $\omega_c[\text{Hz}] = 1.011 \cdot 10^{18} B[\text{T}] E_e^2[\text{GeV}^2]$
$y$		$\hat{=}$ $\omega/\omega_c = \epsilon/\epsilon_c = \lambda_c/\lambda$
$\frac{\Delta\omega}{\omega}$	[%]	$\hat{=}$ bandwidth
$X$		$\hat{=}$ $\gamma\psi$
$\xi$		$\hat{=}$ $\frac{y}{2}(1 + X^2)^{3/2}$
$K_\nu(y)$		$\hat{=}$ modified bessel function of odd order $\nu$

**Tab. 2.1:** Nomenclature of the most important physical constants, abbreviations and substitutions.

## 2.2 Brightness and source emittance

As mentioned in the previous chapter, equation 2.1 implies an ideal i.e. point like electron beam with a negligible emittance (i.e. without any spatial extension). Effects due to finite transverse expansions  $\sigma_{x,y}$  as well as angular divergences  $\sigma'_{x,y}$  of the electron beam must be taken into consideration by means of the storage ring optics (also twiss functions<sup>2</sup> mentioned) in the region of the SR sources (see figures 2.3 and 2.4). Under consumption of an gaussian electron density and angular divergence distribution of the electron beam with

$$\rho(x, x', y, y') = \frac{1}{(2\pi)^2 \sigma_x \sigma'_x \sigma_y \sigma'_y} \exp \left[ -\frac{1}{2} \left( \frac{x^2}{\sigma_x^2} + \frac{x'^2}{\sigma_x'^2} + \frac{y^2}{\sigma_y^2} + \frac{y'^2}{\sigma_y'^2} \right) \right] \quad (2.19)$$

one can determine the first order moments of this normal distribution using the emittance  $\epsilon_{x,y}$  and the energy spread  $\Delta E/E$  of the storage ring as well as the twiss parameter at the source point. The rms-values of the gaussian distribution correspond to the following relations for the beam size and the angular divergence (see fig. 2.2):

$$\sigma_{x,y} = \sqrt{\epsilon_{x,y} \cdot \beta_{x,y} + \left( D_{x,y} \frac{\Delta E}{E} \right)^2}, \quad \sigma'_{x,y} = \sqrt{\epsilon_{x,y} \cdot \frac{1 + \alpha_{x,y}^2}{\beta_{x,y}}} \quad (2.20)$$

For  $\alpha_{x,y} = 0$ , e.g. in the symmetry point of the magnet lattice optics, and neglecting the dispersion term  $D_{x,y}$  one obtains an approximation for the ideal (theoretical) emittance:

$$\epsilon_{x_0, y_0} = \sigma'_{x,y} \cdot \sigma_{x,y} \quad (2.21)$$

At a real machine the strength of the emittance x-y-coupling depends mainly on magnetic fringe field effects as well as position errors of the lattice magnets. It can be expressed by an estimated coupling factor  $\kappa$  which can be controlled by skewed quadrupoles. Usually the factor is in the order of some per cent and an estimation of the 'real' emittance is given by [15, A. Ropert].

$$\epsilon_x = \frac{1}{1 + \kappa} \epsilon_{x_0} \quad \text{respectively} \quad \epsilon_y = \frac{\kappa}{1 + \kappa} \epsilon_{x_0} \quad (2.22)$$

The impact of the finite emittance can be taken into account by folding the photon flux with the gaussian distribution function if the spectral flux density (formular 2.4) can be approximated by the following correction terms:

- Generally, for dipole and wiggler magnets the horizontal divergence of the electron beam can be disregarded ( $\sigma'_x \ll \Theta^{SR} \hat{=}$  opening angle of the synchrotron radiation fan). For this reason, the folding is considered only in the vertical direction resulting in:

$$\frac{d^2 F_B}{d\theta d\psi} \Big|_{\psi=0} = \frac{dF_B}{d\theta} \cdot \frac{1}{4\pi^2 \sqrt{\sigma_\psi^2 + \sigma_y'^2}} \cdot \frac{1}{2\pi \sigma_x \sigma_y} \quad (2.23)$$

with the wavelength depending relation:  $\sigma_\psi \sim 1/\gamma \hat{=}$  natural opening angle of the SR (see equation B.3 resp. B.4). A good approximation for  $\sigma_\psi$  is given by (see also figure

<sup>2</sup>e.g. beta functions  $\beta_{x,y}(s)$ , slope of the beta functions  $\alpha_{x,y}(s) := -\beta'_{x,y}(s)/2$ , dispersion functions  $D_{x,y}(s)$

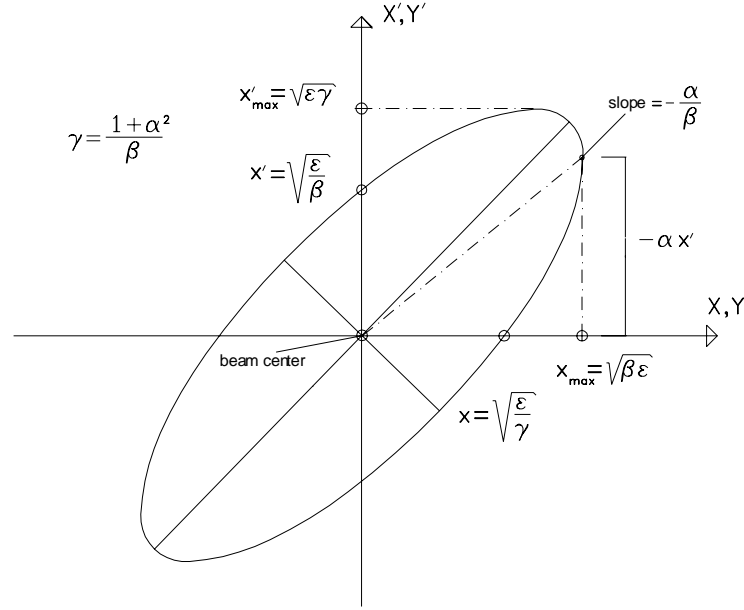


**Fig. 2.2:** Definitions of the emittance ellipse in the phase space.

B.2 in chapter B):

$$\sigma_\psi \approx \frac{2}{\gamma\sqrt{2\pi}} \cdot C(y) = 0.408 \frac{C(y) [\text{mrad}]}{E [\text{GeV}]} \quad (2.24)$$

- In case of the spectral brilliance ('peak brightness'  $B_0$ ) of the undulator radiation basically the emittance of the storage ring optics is the most controlling parameter. In this case the folding must be performed in both directions giving:

$$B_0 \approx \frac{F_{\text{undulator}}}{4\pi^2 \epsilon_x \cdot \epsilon_z} \quad (2.25)$$

Additionally, considering the wavelength dependence of the rms-angular-width of the undulator radiation  $\sigma_{r'} = \sqrt{\frac{\lambda_n}{2L}}$  one gets:

$$B_0 \cong \frac{F_{\text{undulator}}}{2\pi \sqrt{(\sigma_{r'}^2 + \sigma_{x'}^2) \cdot (\sigma_{r'}^2 + \sigma_{y'}^2)}} \quad (2.26)$$

In addition to the specification of each SR source, the corresponding storage ring optics (twiss parameter) are listed separately. Thus, all information are available to estimate the influence of the electron beam parameter (size, angular divergence) on the SR spectra.

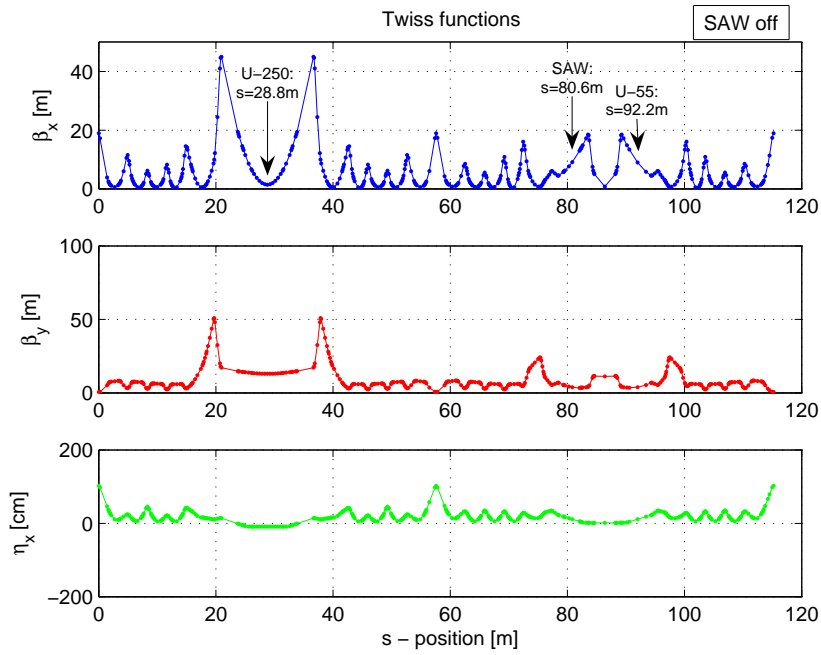


**Fig. 2.3:** Optical functions (betafuncions  $\beta_{x,y}$  and dispersion  $\eta_x$ ) along the orbit position  $s$  (DELTA-008 standard optics; SAW off).

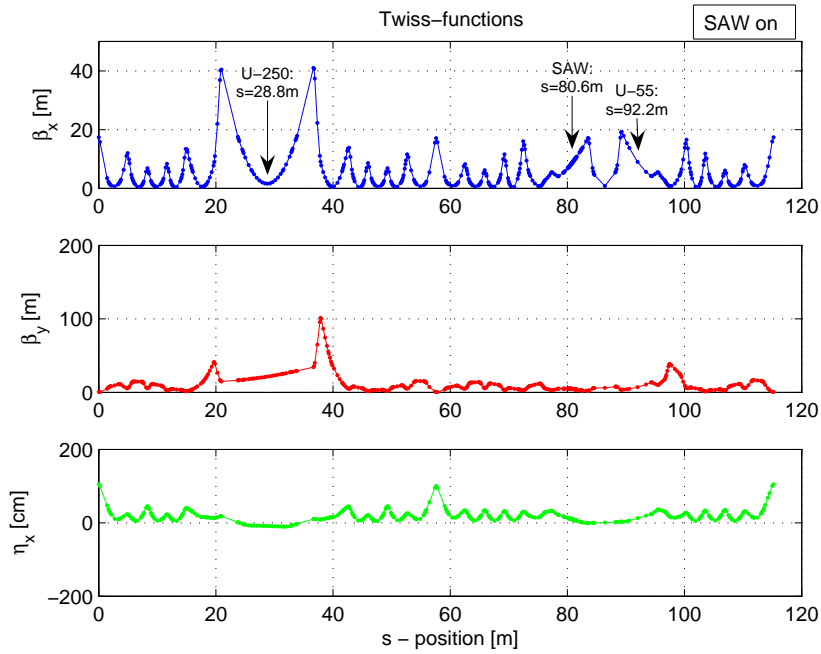


**Fig. 2.4:** Optical functions (betafuncions  $\beta_{x,y}$  and dispersion  $\eta_x$ ) along the orbit position  $s$  (DELTA-008 standard optics; SAW on).

## 2 Calculation of the synchrotron radiation properties

Beamline	s[m]	$\beta_x$ [m]	$\alpha_x$ [rad]	$\psi_x/2\pi$	$\beta_y$ [m]	$\alpha_y$ [rad]	$\psi_y/2\pi$	$D_x$ [m]	$D'_x$ [rad]
BL-0	2,72	0,63	-0,06	0,21	7,85	-0,22	0,19	0,11	-0,10
BL-1	6,62	0,61	0,52	0,53	7,37	0,12	0,30	0,06	0,05
BL-2	9,97	0,63	-0,21	1,02	6,21	0,11	0,40	0,05	-0,06
BL-3	28,79	1,42	0,00	2,29	12,96	0,00	0,74	-0,09	0,00
BL-4	28,79	1,42	0,00	2,29	12,96	0,00	0,74	-0,09	0,00
BL-5	28,79	1,42	0,00	2,29	12,96	0,00	0,74	-0,09	0,00
BL-6	47,61	0,63	0,21	3,55	6,22	-0,11	1,08	0,05	0,06
BL-7	64,21	0,68	0,29	5,10	7,25	0,14	1,77	0,05	0,01
BL-8	80,56	8,16	-1,22	6,63	3,97	0,40	2,20	0,13	-0,05
BL-9	80,56	8,16	-1,22	6,63	3,97	0,40	2,20	0,13	-0,05
BL-10	80,56	8,16	-1,22	6,63	3,97	0,40	2,20	0,13	-0,05
BL-11	92,20	8,16	1,23	7,12	3,98	-0,40	2,56	0,12	0,05
BL-12	108,55	0,68	-0,28	8,65	7,26	-0,14	2,99	0,06	-0,01

**Tab. 2.2:** Twiss parameter (*DELTA-008 optics*) at various beamlines (*BL-0 ... BL-12*).

Beamline	Source	s [m]	$\sigma_x[\mu m]$	$\sigma'_x[\mu rad]$	$\sigma_y[\mu m]$	$\sigma'_y[\mu rad]$
BL-0	Bending Magnet	2.72	120	153	107	14
BL-1	Bending Magnet	6.62	103	175	104	14
BL-2	Bending Magnet	9.97	102	156	95	15
BL-3	FEL	28.79	156	101	138	11
BL-4	FEL	28.79	156	101	138	11
BL-5	U-250	28.79	156	101	138	11
BL-6	Bending Magnet	47.61	103	156	95	15
BL-7	Bending Magnet	64.21	107	152	103	14
BL-8	SAW	80.56	356	67	76	21
BL-9	SAW center	80.56	356	67	76	21
BL-10	SAW	80.56	356	67	76	21
BL-11	U-55 center	92.20	355	67	76	21
BL-12	Bending Magnet	108.55	107	152	103	14

<sup>a</sup>Nominal emittance (@ 1.48 GeV):  $\epsilon_x = 15 \text{ nm}$ ,  $\epsilon_y = 1.5 \text{ nm}$

<sup>b</sup>Energy spread:  $\Delta E/E = 7 \cdot 10^{-7}$

**Tab. 2.3:** Beam size and divergence at various beamlines (*BL-0 ... BL-12*).

## 2.3 Pulsed time structure

The RF system of the storage ring is essential to replenish the radiated SR energy per revolution. Thus, the electron beam is modulated in the longitudinal direction because of the alternating radio frequency (RF) field which is necessary to accelerate the beam. This radiation is pulsed with each electron pulse typically of a few percent of the RF period, whereby the circumference must be a whole-numbered multiple of the RF period (so called harmonic number). These values define the number of discrete bunches of electrons in the storage ring. Consequently the time structure of the SR is determined by:

- the fundamental frequency of the RF cavity,
- the circumference of the storage ring,
- the corresponding harmonic number,
- as well as the number and distribution of the bunches stored in the ring (filling pattern).

Table 2.4 summarizes the actual values for DELTA.

Circumference	[m]	115.2
RF-frequency	[MHz]	500
Harmonic number		115.2 m / 0.6 m = 192
Number of buckets n		192/n = integer number
Revolution time	[ns]	384 (corresponds to 2.6 MHz)
Energy spread $\Delta E/E$		$7 \cdot 10^{-4}$
Pulse length <sup>a</sup>	[ps]	20 (single-bunch) – 40 (multi-bunch)

<sup>a</sup>bunch length of 1 cm correspond to 33 ps pulse length

**Tab. 2.4:** *Data for the pulsed time structure of the synchrotron radiation at DELTA.*

The storage ring DELTA is operated in 'single-bunch-mode' for measurements which require a high time resolution. The time of circulation for a single electron bucket amounts then to 384 ns (revolution frequency 2.6 MHz) with a pulse length of typically 20 ps ( $\simeq 1\%$  of the RF period). The pulse length of the radiation depends strongly on the stored beam current, because the bunch length is a complex function of RF parameter (separatrix of the longitudinal motion in the accelerating RF field) and the impedance of the vacuum chamber. Depending on the filling pattern a range of pulse intervals from 20 ps (single bunch mode with 20 mA) up to 40 ps (multi-bunch-mode with 150 mA) are obtained. The spacing between each light pulse in multi-bunch-mode is 2 ns. In the standard user operation mode DELTA uses a typical 2/3-multi-bunch filling pattern which guarantees high currents and large beam life times. This corresponds to a bunch-train of 128 buckets (192 ns), 2 ns subdivided and a gap of 128 ns in time per circulation (384 ns).



### 3 Dipole Radiation

The main storage ring consist of 16 long (1.1m) dipoles along the arcs and 8 short (0.525 m) dipoles installed in the straight sections of the magnet lattice (see fig.1.1). The synchrotron radiation properties of the dipoles depend mainly on the electron energy  $E$  for a given bending radius  $\rho$ . Whereby the critical wavelength of the photon spectra is determined by the relation (in practical units):

$$\lambda_c[\text{\AA}] \cong 5.59 \frac{\rho}{E^3} \left[ \frac{m}{GeV^3} \right] \simeq 5.7[\text{\AA}] \simeq 2.2[keV] \quad (3.1)$$

The tables 3.1 and 3.2 summarize the most important data.



**Fig. 3.1:** *DELTA dipole magnet.*

Six dipoles of the DELTA lattice are already equipped with special SR-outlet vacuum chambers (BL-0,1,2,6,7,12). Formerly BL-2 was used by the German company Micro Parts and the University of Bonn. At present the Institute for Analytical Sciences (ISAS) in Dortmund operates this beamline and took over the responsibility and support for the infra-red beamline BL-0. BL-6 and BL-7 are occupied by the DELTA machine group for electron beam diagnostics (BL-7) and FEL mirror studies (BL-6). The former TGM-3 beamline of BESSY-I is now operated by the University of Dortmund at the bending magnet beamline BL-12. BL-1 is not in use.

All following spectra are normalized to an electron beam current of 1 mA.

<i>Dipole-Parameter</i>	
bending radius <sup>a</sup>	$\rho = 3.33$ m (@ 1.48 GeV)
field strength <sup>b</sup>	$B = 1.48$ T
<i>average values of the twiss parameters (del008 optics):</i>	
$\langle \beta_x \rangle$	$\approx 0.6$ m
$\langle \beta_y \rangle$	$\approx 7.5$ m
$\langle D_x \rangle$	$\approx 0.1$ m
$\langle  \alpha_x  \rangle$	$\approx 0.2$ rad
$\langle  \alpha_y  \rangle$	$\approx 0.1$ rad

$$^a \rho = \frac{E[\text{GeV}]}{0.3 B_0[\text{T}]}$$

<sup>b</sup>Basic setting during standard user operation;  $B_{max} = 1.51$  T

**Tab. 3.1:** *Bending magnet data.*

E [GeV]	0.5	1.0	1.5
$\gamma^a$	978	1957	2935
$\lambda_c [\text{\AA}]^b$	149	18.5	5.5
$\epsilon_c [\text{keV}]^c$	0.083	0.67	2.26
P [kW] @ 100 mA	0.17	2.7	13.5
$\Delta E [\text{keV}]$	1.67	26.73	135.31
B [T]	0.50	1.01	1.51

$$^a \gamma = E[\text{GeV}]/0.511[\text{GeV}]$$

$$^b \lambda_c [\text{\AA}] = \frac{18.64}{B[\text{T}] \cdot E^2[\text{GeV}^2]}$$

$$^c \epsilon_c [\text{keV}] = 0.665 \cdot B[\text{T}] \cdot E^2[\text{GeV}^2]$$

**Tab. 3.2:** *Characteristic DELTA dipole SR data at different storage ring energies.*

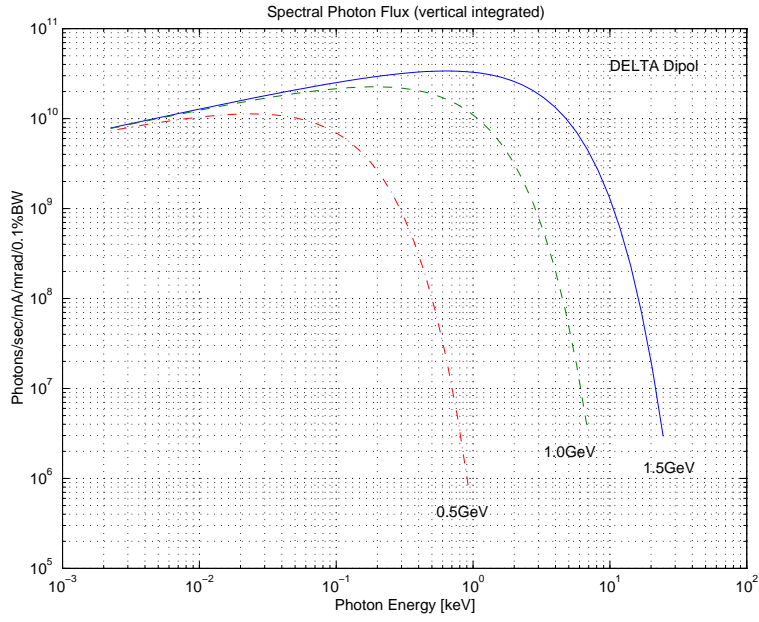


**Fig. 3.2:** Vertical integrated photon flux (number of photons at a given wavelength/energy within a given bandwidth, integrated over all vertical opening angles) for different storage ring energies.

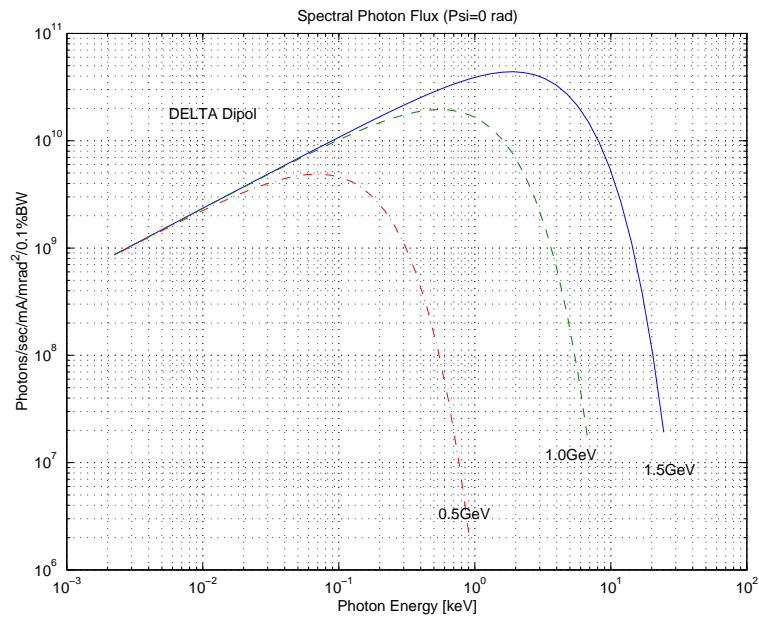


**Fig. 3.3:** Photon flux in the median plane ( $\psi = 0$ ) for different storage ring energies.

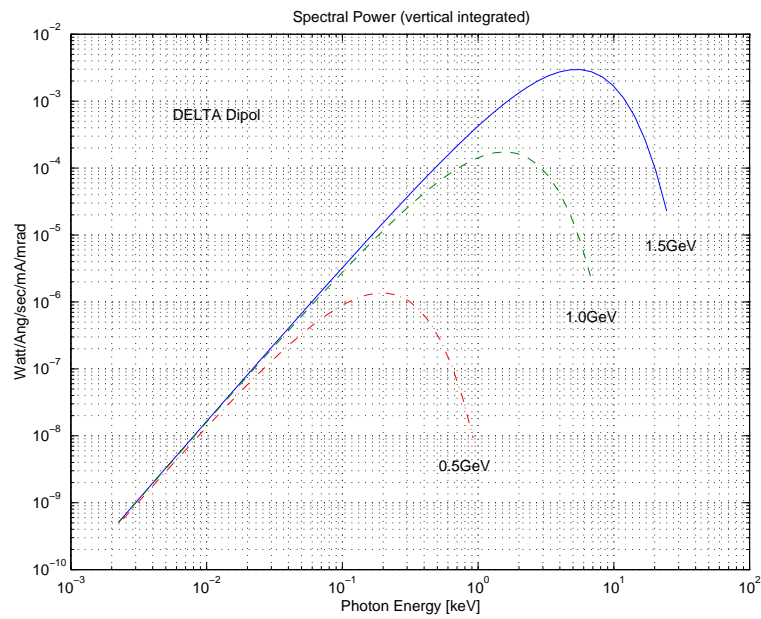


**Fig. 3.4:** Spectral distribution of the radiated power (vertical integrated) for different storage ring energies.

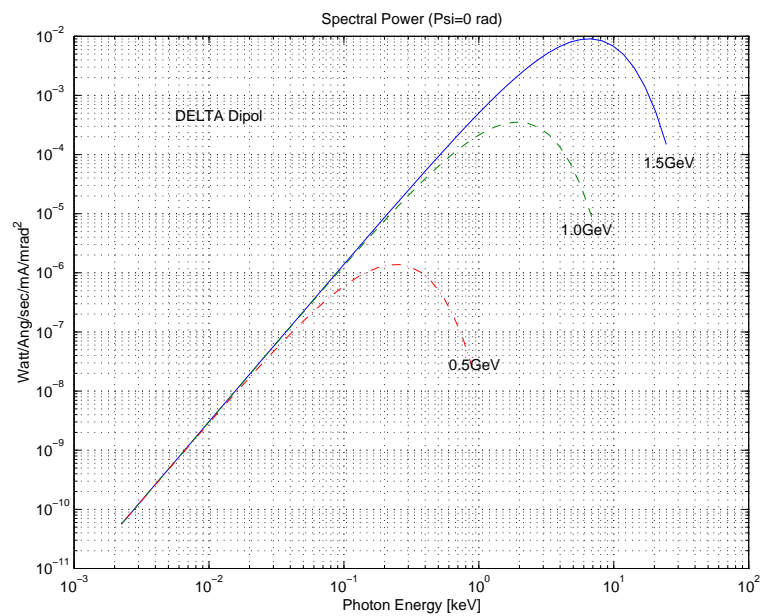


**Fig. 3.5:** Spectral power in the median plane ( $\psi = 0$ ) for different storage ring energies.

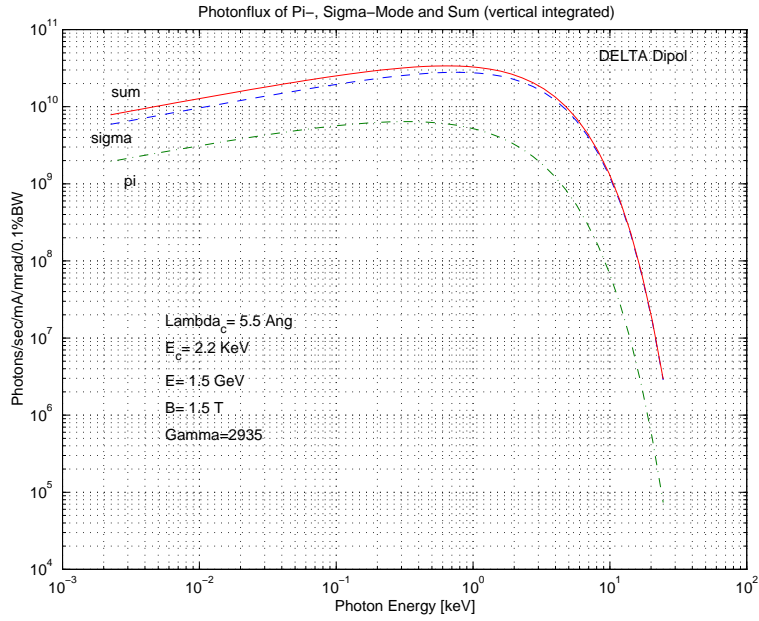


**Fig. 3.6:** Vertical integrated spectral photon flux distribution of the parallel (*sigma*) and perpendicular (*pi*) components of the electric field vector with respect to the orbit plane (@1.5GeV).

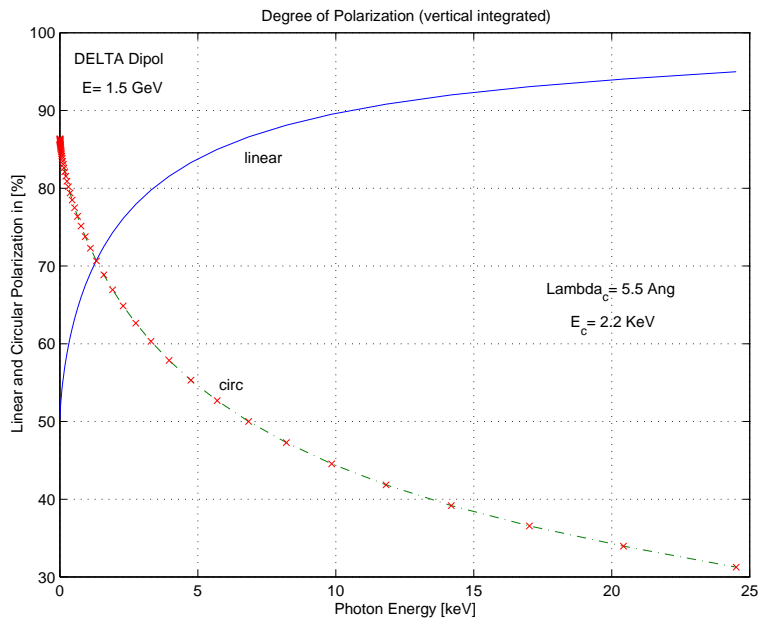


**Fig. 3.7:** Degree of linear and circular polarization as a function of photon energy.

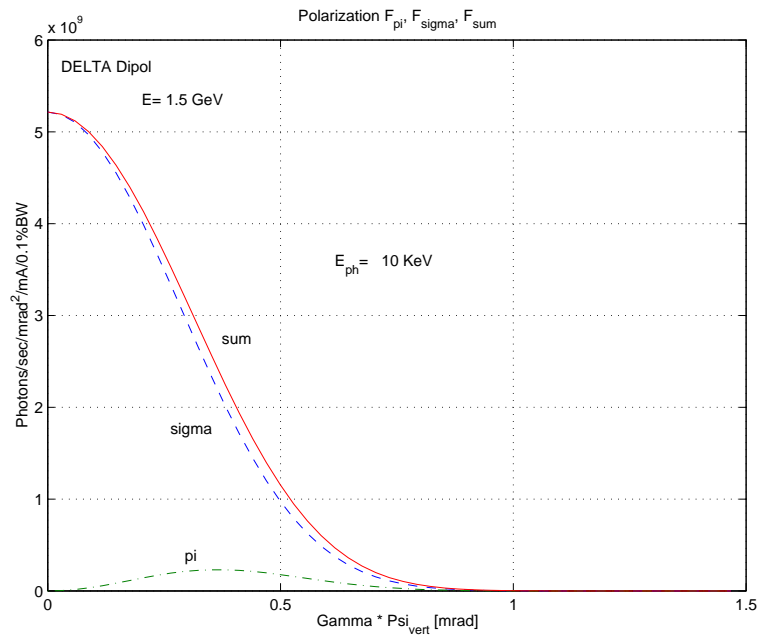


**Fig. 3.8:** Vertical angular distribution of parallel ( $\sigma$ ) and perpendicular ( $\pi$ ) polarization components (for 10 keV photons).

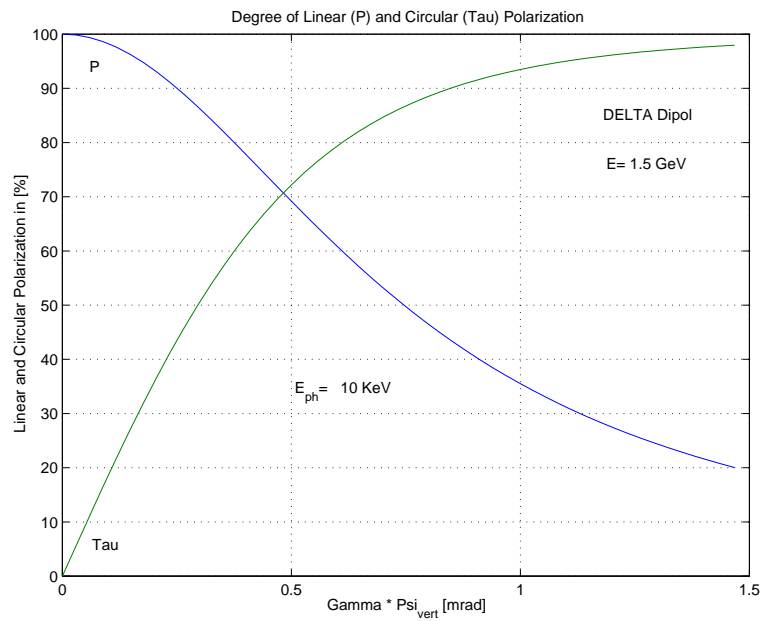


**Fig. 3.9:** Linear and circular polarization as a function of the vertical emission angle (for 10 keV photons)

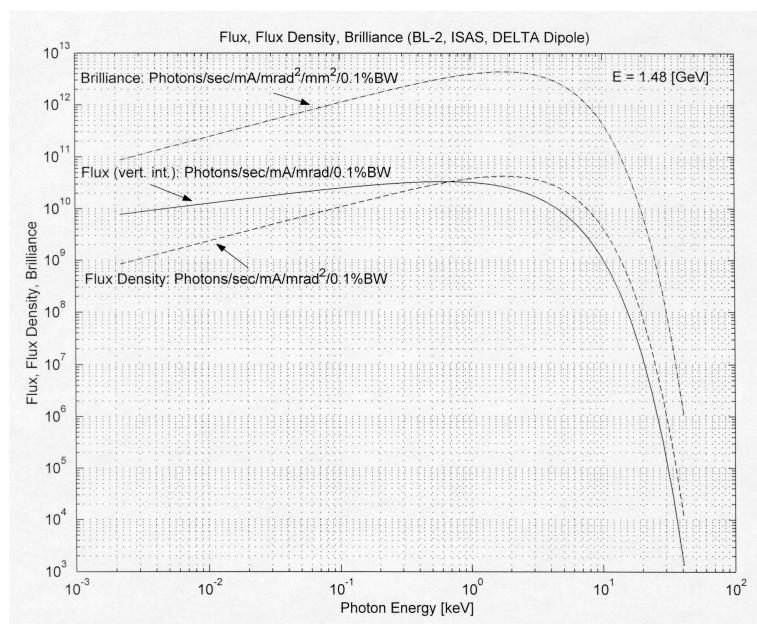


**Fig. 3.10:** Flux, flux density and brilliance generated by a DELTA bending magnet (here @ ISAS BL-2). DELTA beam current: 1mA



## 4 SAW Radiation

This chapter summarizes the properties of the synchrotron radiation emitted by the superconducting asymmetric wiggler magnet (SAW) a novel insertion device at DELTA. After several design studies concerning SR spectra and interaction with the storage ring [16], finally the wiggler was manufactured by the German company ACCEL [8]. A special coil arrangement consisting of NbTi-wires allows two operational modes:

- symmetrical: with a sine-like field of 10 periods with a peak field of 2.7 Tesla
- asymmetrical: with 5 periods and a peak value of 5.3 Tesla



**Fig. 4.1:** *Superconducting Asymmetric Wiggler (SAW).*

Some wiggler parameters are compiled in table 4.1 [8]. Field investigations have been performed by calibrated hall probe and pulsed wire measurements [8],[17]. As one example, plot 4.2 shows the magnetic field distribution along the complete wiggler magnet axis at full and 40% excitation in the asymmetric mode [18]. Table 4.2 summarizes the peak field numbers at intermediate values of excitation in both modes. More detailed technical descriptions of the SAW can be found in [19],[20],[21],[22].

To avoid major problems with the complex NbTi-wiring in combination with strong magnetic forces and high saturation effects inside the iron yokes, it was required to simplify the technical layout of the SAW. For these engineering reasons it was necessary to modify the arrangement and the wiring of the superconducting NbTi-coils in comparison to the theoretical concept which was optimized to generate a high degree of circular polarized synchrotron radiation. Consequently it was also essential to recalculate all wiggler spectra based on the

Wiggler Parameter [8]	sym. mode	asym. mode
Max. magnetic field	2.79 T	5.30 T
Period length	14.4 cm	28.8 cm
Number of periods	10	5
K-values <sup>a</sup>	38	143
Opening of the light cone <sup>b</sup>	±6.4 mrad	±24 mrad
Critical photon energy <sup>c</sup>	4.2 keV (2.97 Å)	7.9 keV (1.56 Å)
Total length	2.50 m	
Magnetic length	1.44 m	
Full pole gap	18 mm	
Vacuum gap	10 mm (semi-cold)	
Vacuum chamber width	90-120 mm (beam entry - beam exit)	
Chamber temperature	<20 K	
Total weight (without helium)	2250 kg	

$$^a K = \frac{e B_0 \lambda_w}{2 \pi m_e c} = 0.934 \cdot \lambda[cm] \cdot B[T]$$

$$^b \theta_{max}^{SR} \simeq K/\gamma \quad (\gamma = 2935 @ 1.5 GeV)$$

$$^c \epsilon_c[keV] = 0.665 \cdot B[T] \cdot E^2[GeV^2]$$

**Tab. 4.1:** Main wiggler parameter.

real magnetic field measurements because the differences between design and real magnetic field properties are significant. Figure 4.3 shows the theoretical optimized (ideal modelled) and the measured (FFT fit of ACCEL data) magnetic field of the wiggler magnet in the so called 'asymmetric mode' at maximum excitation of 5.3 Tesla. The differences are conspicuous at the weaker positive magnetic field components most evident in the center (144 mm) of the period. This deviation has an important influence on the polarization rate of the SR as explained later.

Corresponding to the rather complicated magnetic field distribution a rather complicated spectra is expected too. To examine these spectra first one has to calculate the equation of motion of an relativistic single electron propagating along the wiggler axis (relativistic Lorentz equation). Two methods have been used to solve the ordinary differential equation (ODE) [23]:

- Numerical integration using the Runge-Kutta-Algorithm and
- FFT-analysis of the periodic magnetic field to calculate the fourier coefficients resulting in an expression which can be integrated analytically.

For crosscheck reasons both methods have been combined.

The plots in figure 4.4 show the first and second magnetic field integrals giving the electron position along the wiggler axis and the gradient angle (angular deflection) of the electron motion. The strong field of 5.3 T leads to a rather large opening angle of approx. ±24 mrad and an orbit offset of approx. 2.3 mm. For large values of the wiggler parameter K ( $K \gg$

---

	symmetric	asymmetric
Excitation	on axis with calibrated hall probe	on axis with pulsed wire method
[%]	[T]	[T]
20	1.1	1.6
40	1.4	2.45
60	1.8	3.2
80	2.2	4.35
100	2.7	5.3

---

<sup>a</sup>Data by ACCEL [18]

**Tab. 4.2:** *Peak field at various coil excitations for the symmetric and asymmetric SAW mode.*

1), the so called classical 'wiggler limit', the fractions of the photon flux from different parts of the electron trajectory are adding up incoherently. Thus the angular spectral flux distribution arise from the superposition of the dipole like radiation from each source point of the electron track. Hence, the SR calculation is reduced to the Schwinger-Formular (see equation 2.4).

Plotting the magnetic field versus the horizontal angular deflection illustrates that for each horizontal emission angle two B-field components per wiggler period must be superposed<sup>1</sup>. The sum of the photon flux (horizontal and vertical polarized) of each contribution ( $B_{pos}$ ,  $B_{neg}$ ) gives the final result which is not the same as the flux for the sum of the B-fields (see picture 4.6).

At a deflection angle of 0 mrad, which corresponds to the source point of the photon flux for the center beamline-9, a B-field of -5.3 T and +2.3 T are contributing. One should notice that in the ideal case the positive component would vanish [23]. As an example figure 4.7 shows the total photon flux (vertical integrated) of 10 keV photons in dependence of the horizontal deflection angle. The strong negative B-field component is continuously decreasing and partly compensated by the increasing positive B-field component at larger horizontal deflection angles (>12 mrad). Due to this effect one identifies the 'shoulder like' progression of the intensity function which depends strongly on the photon energy. Generally, for smaller photon energies the less strong positive B-field becomes more dominant, reflecting also in the degree of linear and circular polarization (see also plot 4.5). The maximum degree of circular polarization of approximately 62% is reached at 12 mrad. Because of the non-ideal magnetic field distribution the maximum degree of circular polarization at 0 mrad (center beamline 9) for 10 keV Photons is 42% (vert. int.) which is considerable reduced in comparison to the ideal case of 62%. The vertical dependences of the photon flux and polarization is similar to a strong dipole (or a superposition of dipoles) and are summarized in the diagrams (4.14 - 4.18). The spectral photon flux properties in dependence of the vertical emission direction are comparable to a strong dipole radiation too. All following figures summarize these properties

---

<sup>1</sup>One notice:  $\text{Flux}(B_1) + \text{Flux}(B_2)$  do not correspond to  $\text{Flux}(B_1 + B_2)$

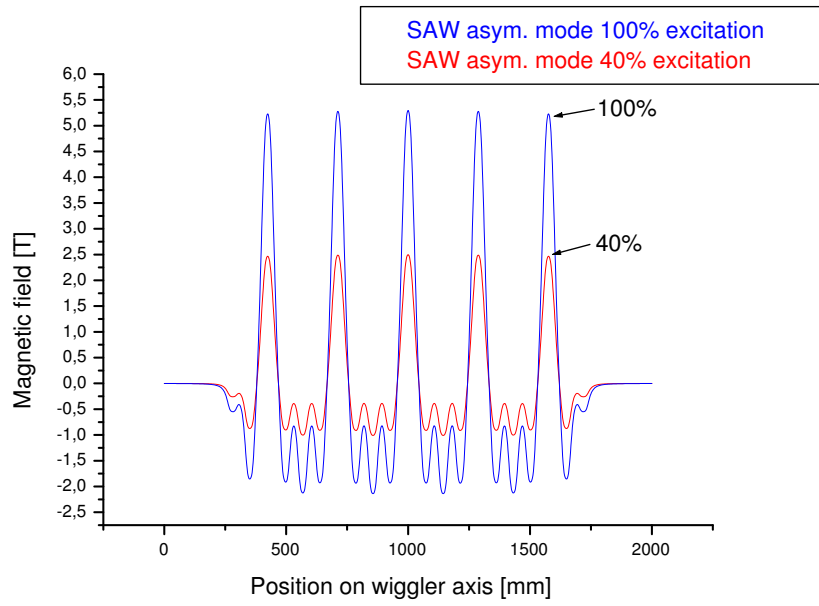


**Fig. 4.2:** Vertical magnetic field component along the wiggler axis (full wiggler length).

of the SAW synchrotron radiation applying to the measured magnetic field distribution with 100% magnetic field excitation in the asymmetrical mode.

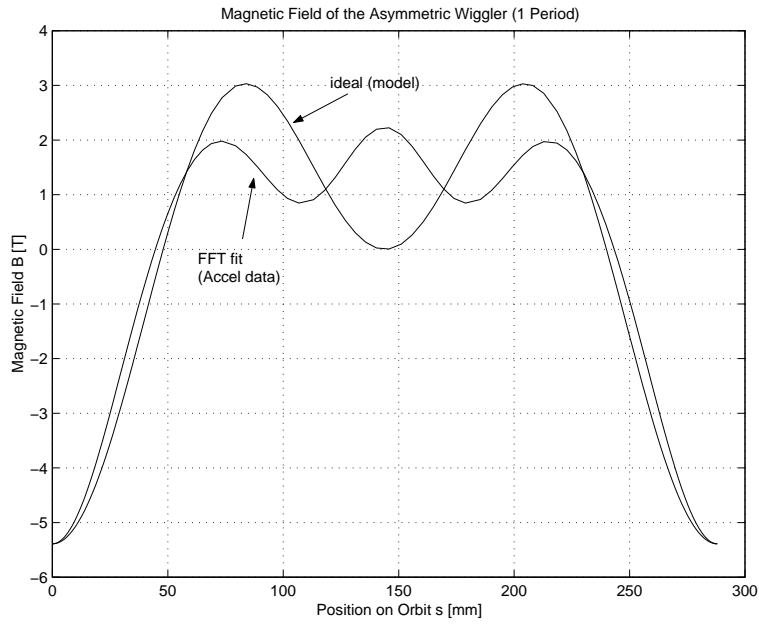


**Fig. 4.3:** Vertical magnetic field component along the wiggler axis (one asymmetric period). Comparison of FFT fit of the measured data [8] and the theoretical optimized model [22].

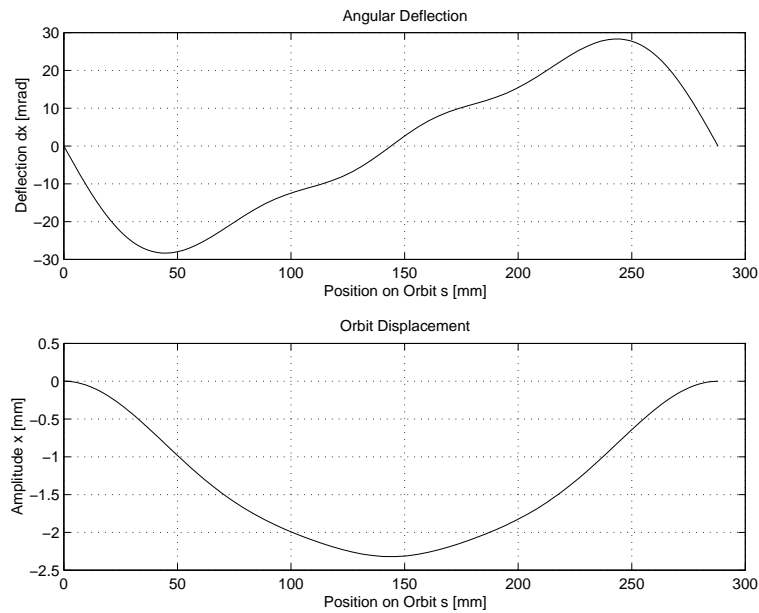


**Fig. 4.4:** Angular deflection and orbit displacement along the wiggler axis (here for measured data).

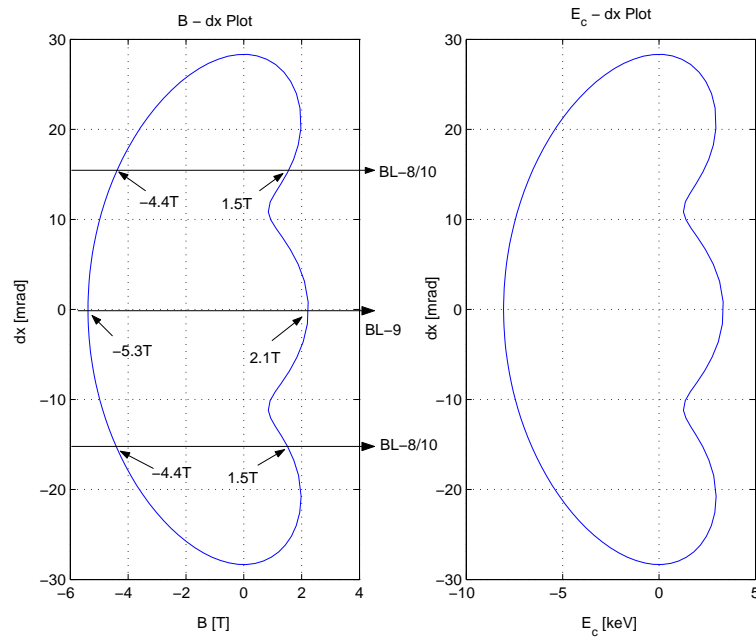


**Fig. 4.5:** Parametric plot of deflection angle vs. magnetic field respectively critical photon energy.

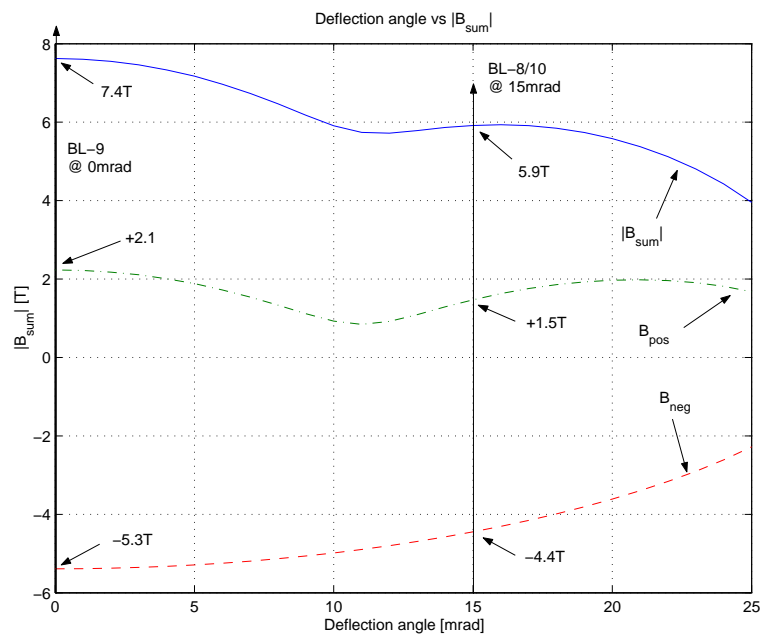


**Fig. 4.6:** Magnetic field contributions from the positive and negative magnetic field components.

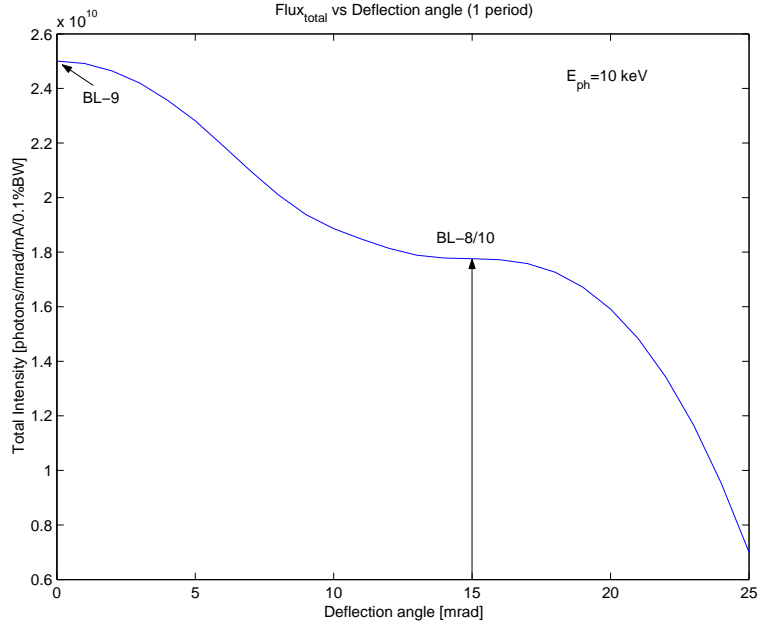


**Fig. 4.7:** Total photon flux versus horizontal deflection angle (here:  $E_{ph} = 10$  keV and one wiggler period).

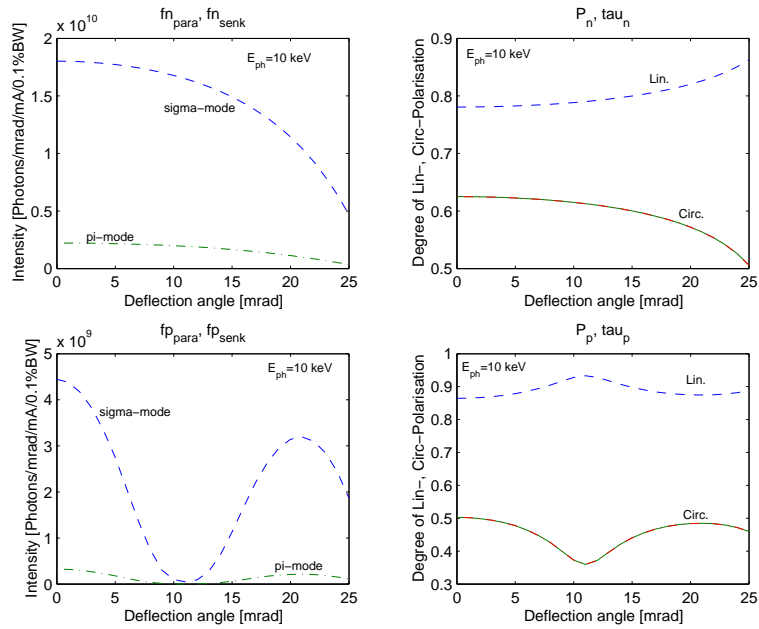


**Fig. 4.8:** Photon flux ( $\sigma$ - and  $\pi$ -mode) and degree of polarization generated by the negative and positive magnetic field components (here:  $E_{ph} = 10$  keV and one wiggler period).

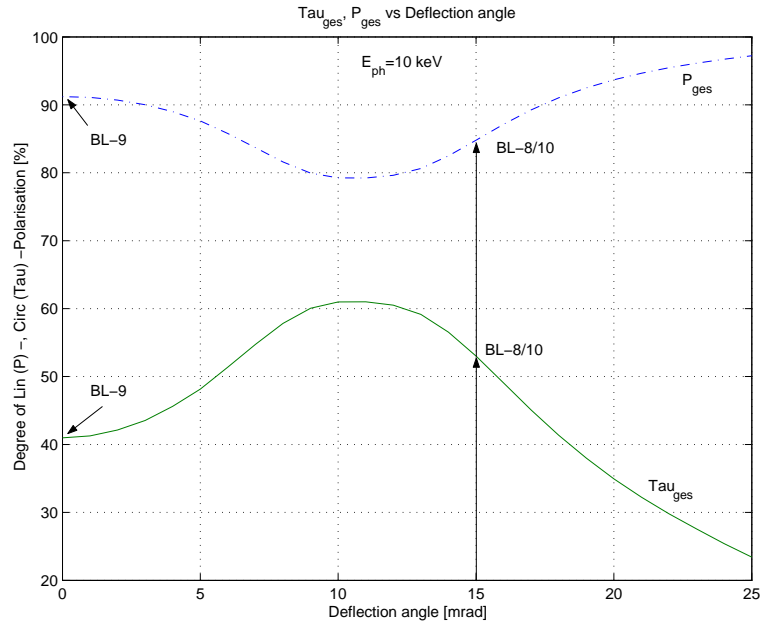


**Fig. 4.9:** Degree of linear ( $P$ ) and circular ( $Tau$ ) polarization in dependence of the horizontal deflection angle (here:  $E_{ph} = 10 \text{ keV}$  and one wiggler period).

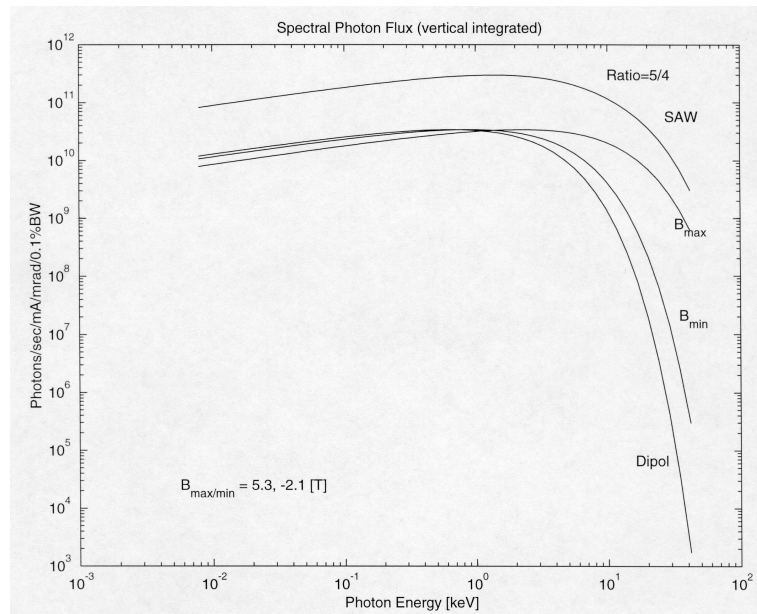


**Fig. 4.10:** Spectral photon flux (vertical integrated) for the center SAW BL-9. Superposition of 5 strong (5.3 T) and 4 weak (-2.1 T) SAW magnetic field components. The DELTA dipole radiation is shown for comparison.

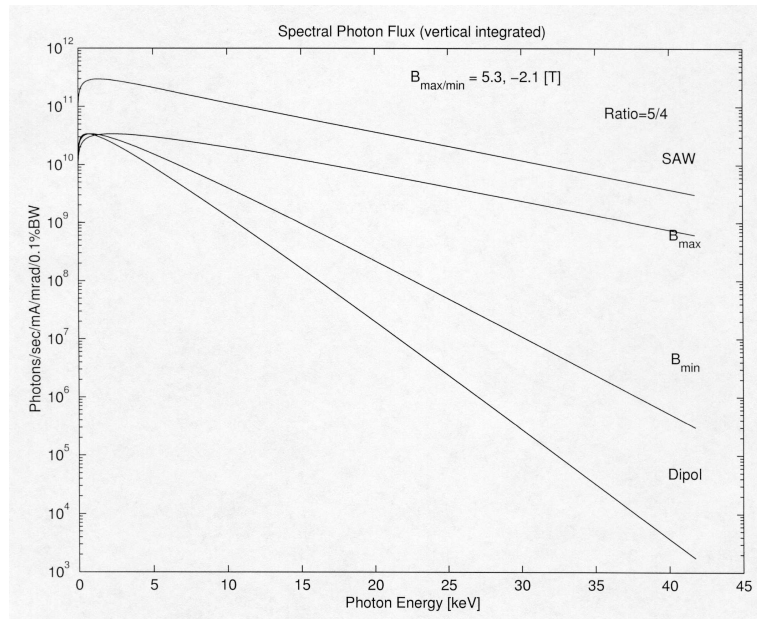


**Fig. 4.11:** Analogous to figure 4.10. Here emphasis on the X-ray range of the spectrum.

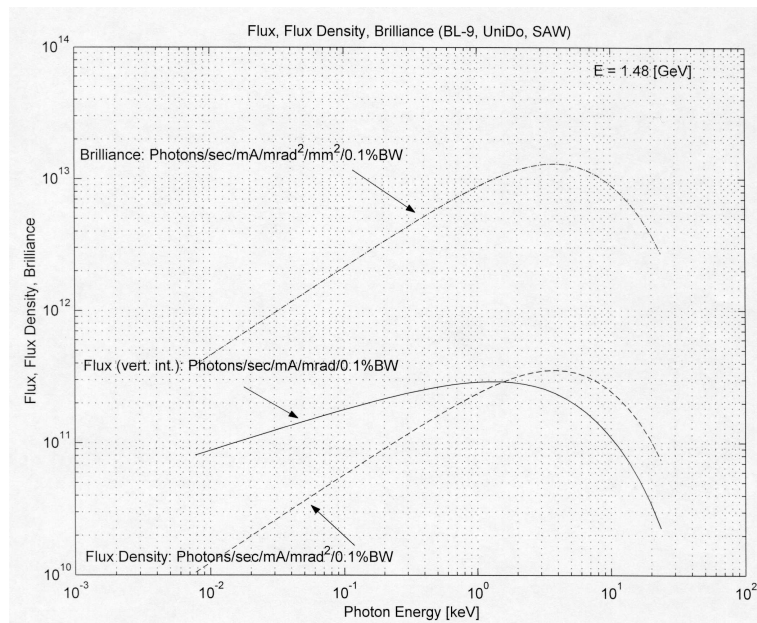


**Fig. 4.12:** Photon flux , flux density and brilliance for the center SAW BL-9.

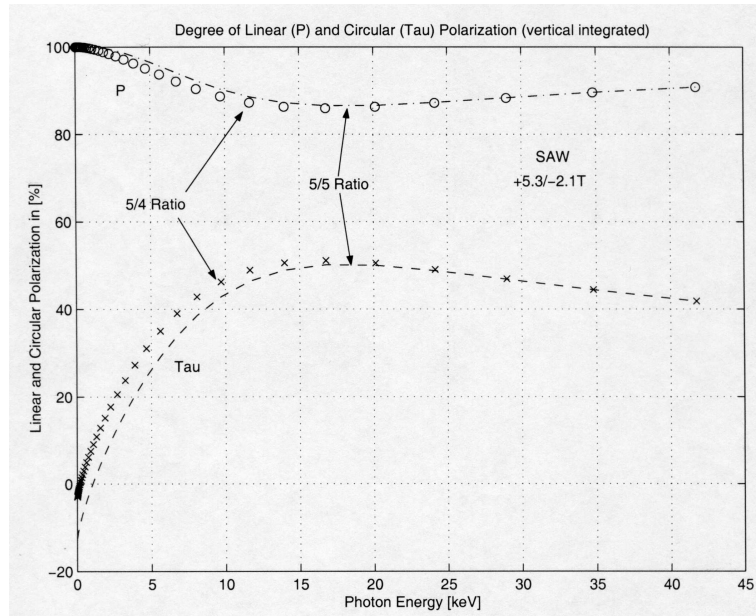


**Fig. 4.13:** Degree of linear (*P*) and circular (*Tau*) polarization in dependence of the photon energy for the center SAW BL-9.

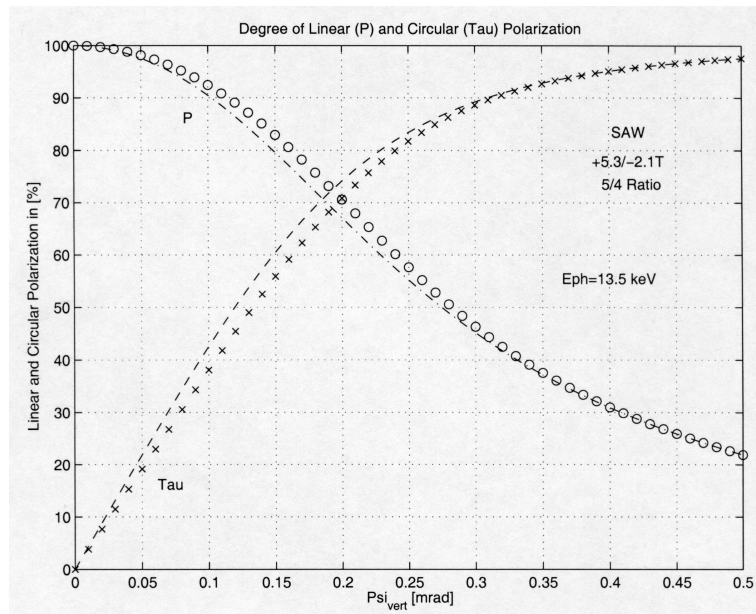


**Fig. 4.14:** Degree of linear (*P*) and circular (*Tau*) polarization for a photon energy of 13.5 keV in dependence of the vertical emission angle (center SAW BL-9).

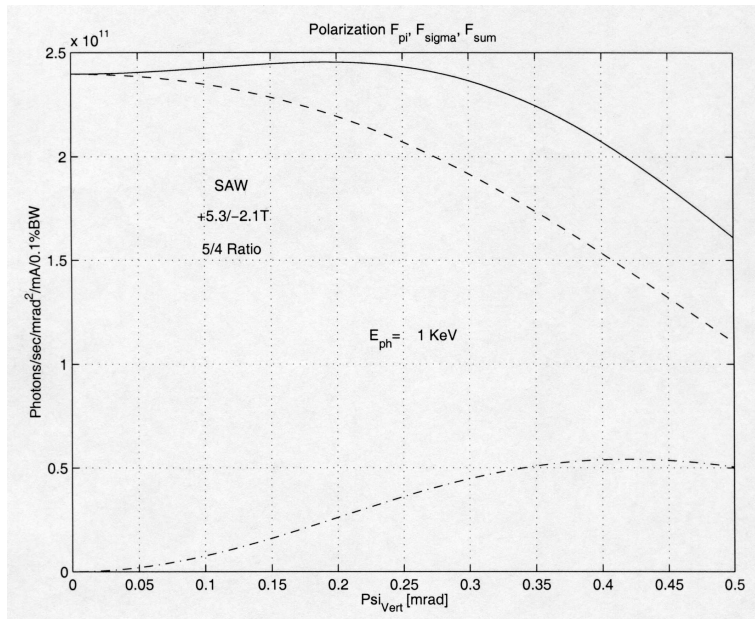


**Fig. 4.15:** Vertical angular distribution of parallel ( $\sigma$ ) and perpendicular ( $\pi$ ) polarization components (photon flux for 1 keV photons) (center SAW BL-9).

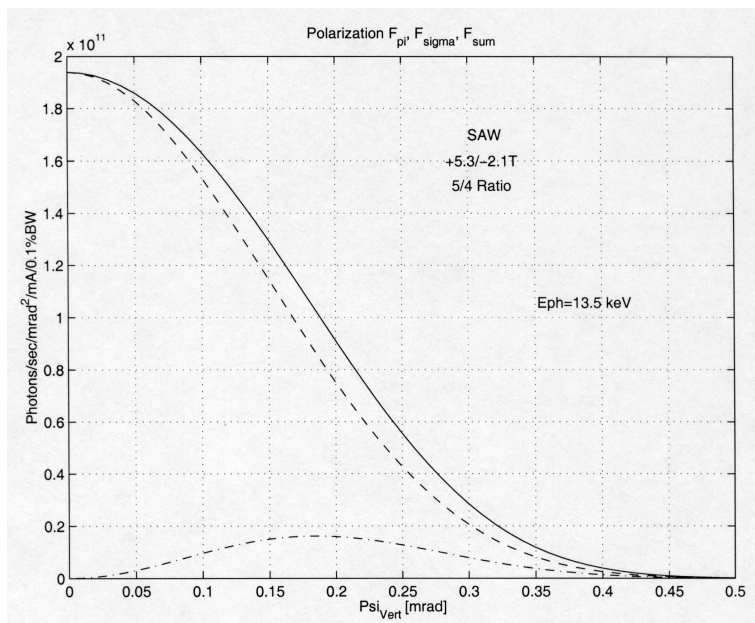


**Fig. 4.16:** Vertical angular distribution of parallel ( $\sigma$ ) and perpendicular ( $\pi$ ) polarization components (photon flux for 13.5 keV photons) (center SAW BL-9).

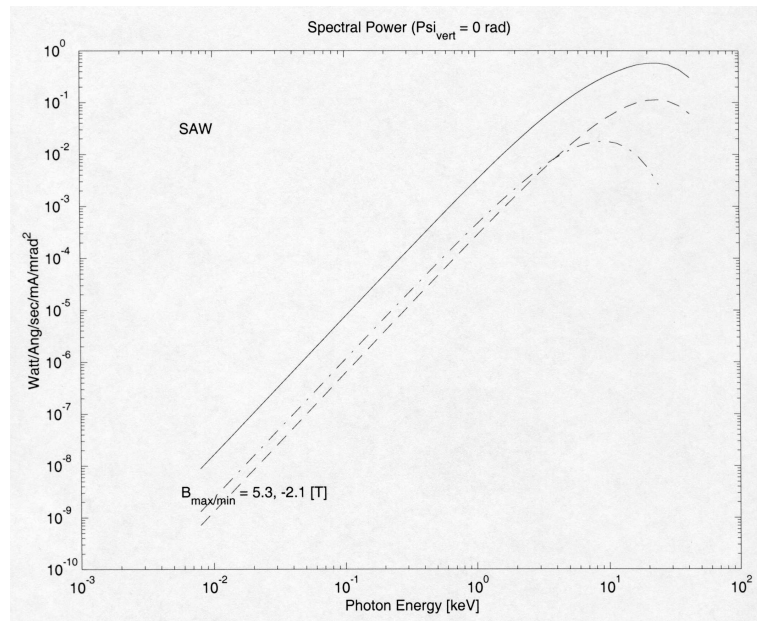


Fig. 4.17: Spectral power in the median plane ( $\psi = 0$ ) (center SAW BL-9).

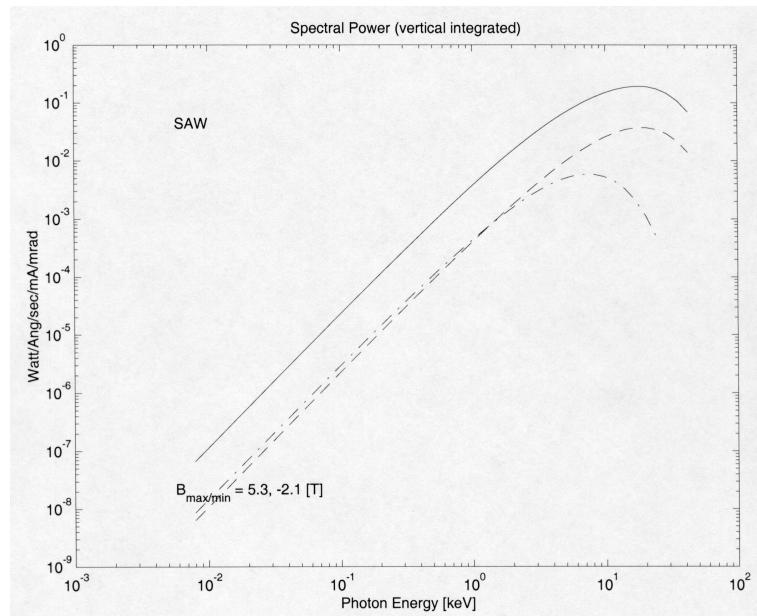
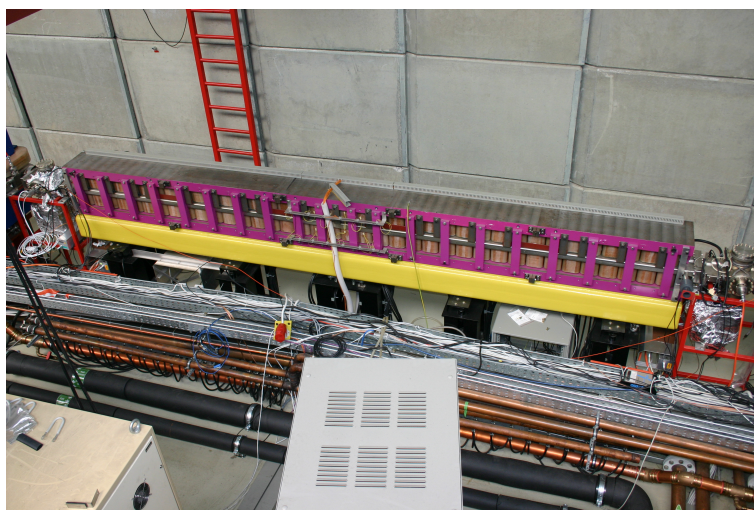


Fig. 4.18: Spectral distribution of the radiated power (vertical integrated) (center SAW BL-9).

## 5 Undulator Radiation

### 5.1 U-250

The undulator for the FEL experiment FELICITA-I has been installed at the final position in the storage ring DELTA in spring 1995. Detailed magnetic measurements have been performed to get a complete characterization of this device in both possible modes, pure undulator and optical klystron mode, respectively. The on-axis magnetic field was measured using both a hall probe and the pulsed-wire technique. Both measurements show good agreement [24],[25].



**Fig. 5.1:** *Electromagnetic undulator U250.*

The electromagnetic undulator has a period length of 25 cm and its overall length is 4.875m, the full height of the fixed gap measures 50 mm. With the power supplies currently used the undulator can provide a maximum K-value of 3.06 with an relative error of about  $10^{-3}$ . As the design of the coils of the dispersion section and the undulator sections is identical the whole undulator can be powered up to a resulting K-value of about 16. The following tables and illustrations summarize the most important data and spectra. Detailed discussions and derivations of the undulator radiation formulas are described for example in [14], [26]. Essential formulas (in practical units) are appended as footnotes to the corresponding insertion device parameter tables.

<i>U-250 Parameter</i>	<i>FEL-mode</i>	<i>Undulator-mode</i>
max. field	$B_0 = 91 \text{ mT}$	$B_0 = 131 \text{ mT}$
bending radius <sup>a</sup>	$\rho = 55 \text{ m} (@1.5\text{GeV})$	$\rho = 38.2 \text{ m} (@1.5\text{GeV})$
period length	$\lambda_u = 250 \text{ mm}$	$\lambda_u = 250 \text{ mm}$
number of periods	$N_P = 17$	$N_P = 17$
undulator parameter <sup>b</sup>	$K = 2.12$	$K = 3.06$
gap	$50 \text{ mm}$	$50 \text{ mm}$
total length	$L = 4.875 \text{ m}$	$L = 4.875 \text{ m}$
first harmonic $\epsilon_1^c$	$26.3 \text{ eV} (471 \text{ nm})$	$15.1 \text{ eV} (824 \text{ nm})$
<i>average values of the twiss parameters (del008 optics):</i>		
$\langle \beta_x \rangle$		$\approx 1.5 \text{ m}$
$\langle \beta_y \rangle$		$\approx 13 \text{ m}$
$\langle D_x \rangle$		$\approx -0.1 \text{ m}$
$\langle  \alpha_x  \rangle$		$\approx 0 \text{ rad}$
$\langle  \alpha_y  \rangle$		$\approx 0 \text{ rad}$

$$^a \rho = \frac{E[\text{GeV}]}{0.3 B_0[\text{T}]}$$

$$^b K = \frac{e B_0 \lambda_u}{2 \pi m_e c} \approx 0.934 \cdot \lambda_u[\text{cm}] \cdot B_0[\text{T}]$$

$$^c \epsilon_1[\text{keV}] = 0.95 \frac{E^2[\text{GeV}^2]}{(1+K^2/2) \cdot \lambda_u[\text{cm}]} ; \quad \lambda_1[\text{\AA}] = \frac{13.056 \cdot \lambda_u[\text{cm}]}{E^2[\text{GeV}^2]} \cdot (1 + K^2/2 + \gamma^2 \Theta^2) \text{ here: on axis } (\Theta = 0)$$

**Tab. 5.1:** Main data of the electromagnetic FEL undulator magnet U-250 (@1.5GeV).

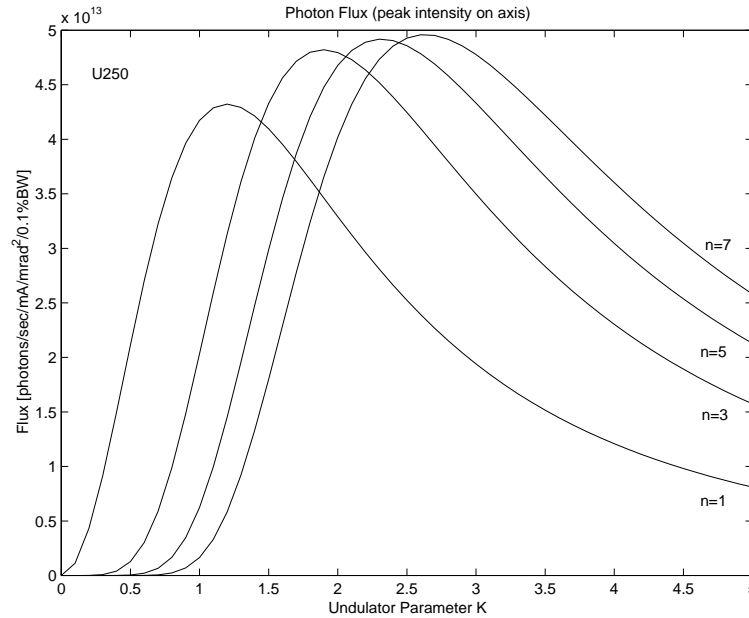


**Fig. 5.2:** Photon flux (peak intensity on axis) versus undulator parameter  $K$  for various harmonic numbers (1,3,5,7). DELTA: ( $E=1.5\text{GeV}$ ;  $I=1\text{mA}$ ).

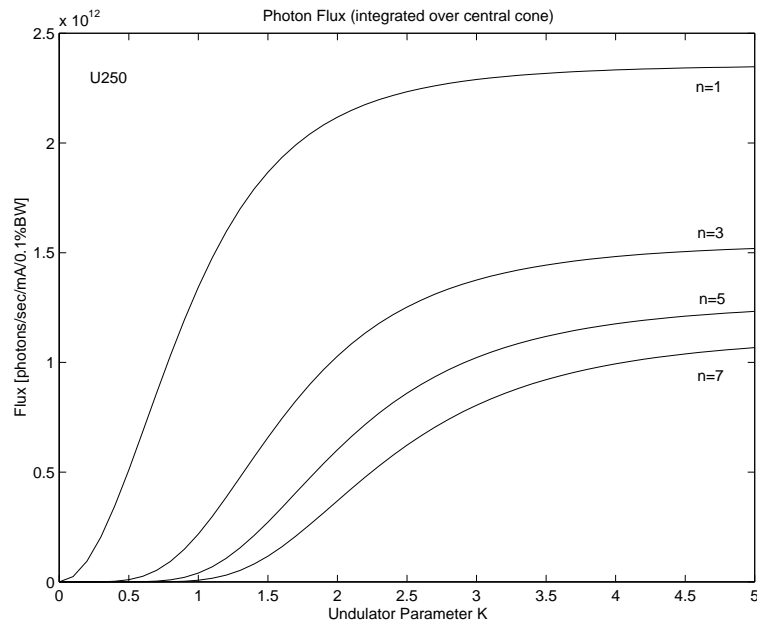


**Fig. 5.3:** Photon flux (integrated over central cone) versus undulator parameter  $K$  for various harmonic numbers (1,3,5,7). DELTA: ( $E=1.5\text{GeV}$ ;  $I=1\text{mA}$ ).

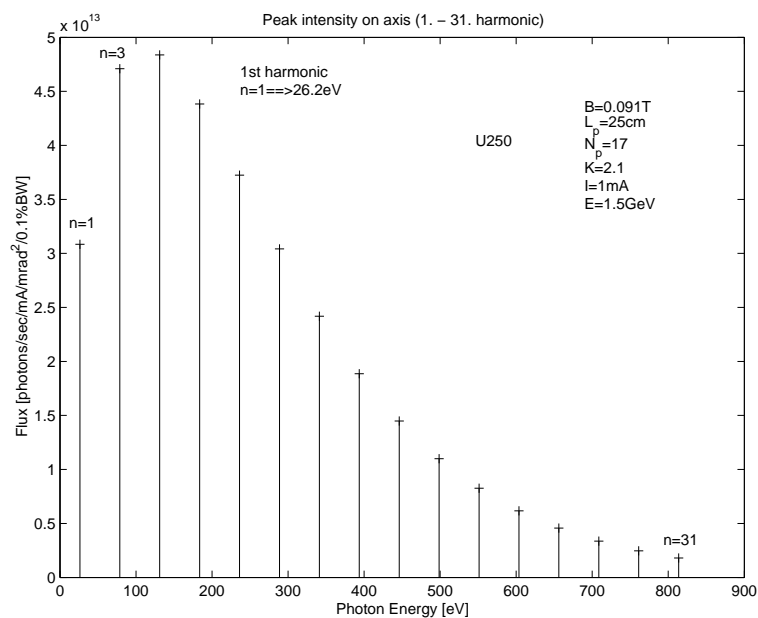


**Fig. 5.4:** Photon flux (peak intensity on axis) versus photon energy (corresponding odd harmonic numbers 1-31). DELTA: ( $E=1.5\text{GeV}$ ;  $I=1\text{mA}$ ).

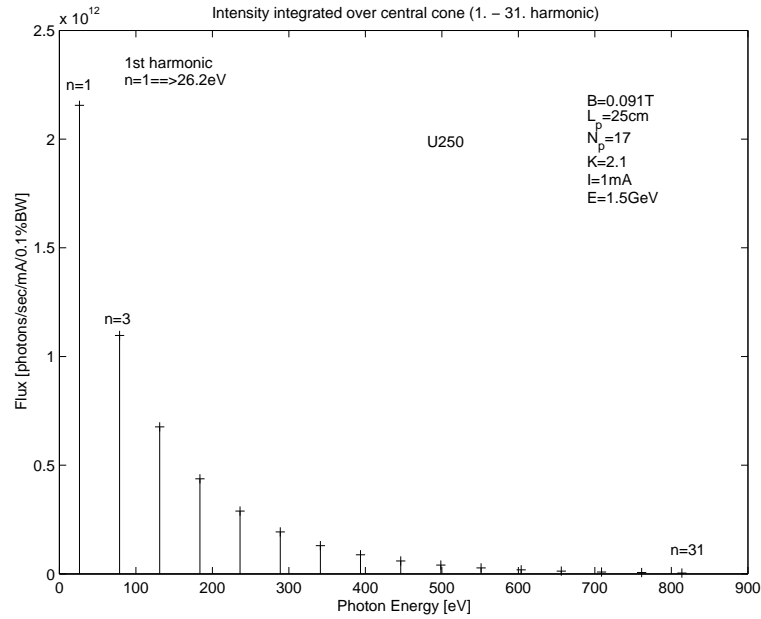


**Fig. 5.5:** Photon flux (integrated over central cone) versus photon energy (corresponding odd harmonic numbers 1-31). DELTA: ( $E=1.5\text{GeV}$ ;  $I=1\text{mA}$ ).

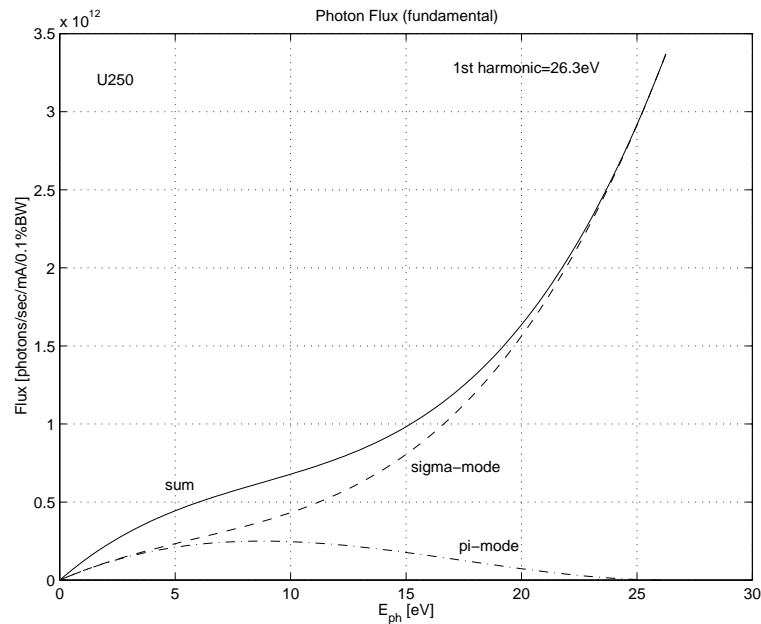


**Fig. 5.6:** Photon flux (fundamental=26.3eV) versus photon energy  $E_{ph}$ , (horizontal (sigma-mode) and vertical (pi-mode) polarized). DELTA: ( $E=1.5\text{GeV}$ ;  $I=1\text{mA}$ ).

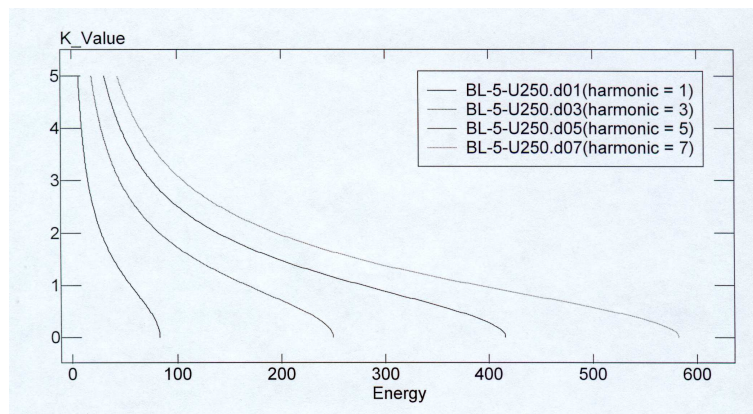


**Fig. 5.7:** Undulator parameter  $K$  versus photon energy  $E_{ph}$  for various harmonic numbers (1,3,5,7), DELTA: ( $E=1.5\text{GeV}$ ;  $I=1\text{mA}$ ).

## 5.2 U-55

The hybrid undulator U55 was built by the German company ACCEL [8] and has been installed in 1999. The insertion device is a representative of a classical hybrid undulator type with a combination of iron poles excited by permanent NdFeB-magnets. The device consists of 97 poles (95 full field) made of pure ARMCO iron with a remanent magnetic flux density of min. 1.15 T (1.2 T nominal measured @20°C). The gap can be varied from min. 20 mm up to max. 300 mm. The dependence of the peak field in the median plane as a function of gap height is approximately given by [27],[28]:

$$B_{orbit} \cong 1.4 \cdot B_{pole} \cdot e^{-\pi \cdot gap / \lambda_u} \quad (5.1)$$

Where  $B_{pole}$  is the magnetic field at the iron pole generated by the permanent magnets ( $SmCo_5 \simeq 0.95 T$  or  $NdFeB \simeq 1.1 T - 1.2 T$ ) and  $\lambda_u$  is the period length of the undulator. The main parameters of the U55 magnet are summarized in table 5.2. The following tables and illustrations summarize the most important data and spectra.



**Fig. 5.8:** Permanent magnets undulator U55.

<i>U-55 Parameter</i>	
max. field in median plane	$B_0 = 0.68 \text{ T}$ (measured at min. gap of 20 mm)
bending radius <sup>a</sup>	$\rho = 7.4 \text{ m}$ (@ 1.5 GeV)
period length	$\lambda_u = 5.5 \text{ cm}$
number of periods	$N_P = 48$
undulator parameter <sup>b</sup>	$K = 3.5$ (@ gap of 20 mm)
total magnetic length	$L = 2.71 \text{ m}$
first harmonic <sup>c</sup>	$54.7 \text{ eV}$ (227 nm)
<i>average values of the twiss parameters (del008 optics):</i>	
$\langle \beta_x \rangle$	$\approx 8.2 \text{ m}$
$\langle \beta_y \rangle$	$\approx 4 \text{ m}$
$\langle D_x \rangle$	$\approx 0.1 \text{ m}$
$\langle  \alpha_x  \rangle$	$\approx 1.2 \text{ rad}$
$\langle  \alpha_y  \rangle$	$\approx -0.04 \text{ rad}$

$$^a \rho = \frac{E[\text{GeV}]}{0.3 B_0[\text{T}]}$$

$$^b K = \frac{e B_0 \lambda_u}{2 \pi m_e c} \approx 0.934 \cdot \lambda_u[\text{cm}] \cdot B_0[\text{T}]$$

$$^c \epsilon_{1}[\text{keV}] = 0.95 \frac{E^2[\text{GeV}^2]}{(1+K^2/2) \cdot \lambda_u[\text{cm}]} ; \quad \lambda_1[\text{\AA}] = \frac{13.056 \cdot \lambda_u[\text{cm}]}{E^2[\text{GeV}^2]} \cdot (1 + K^2/2 + \gamma^2 \Theta^2) \text{ here: on axis } (\Theta = 0)$$

**Tab. 5.2:** Parameters of the U-55 hybrid undulator.

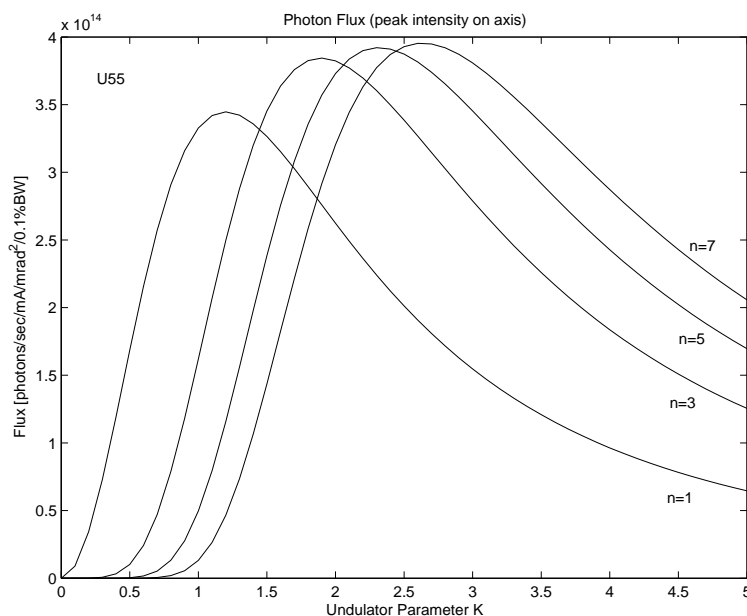


**Fig. 5.9:** Photon flux (peak intensity on axis) versus undulator parameter  $K$  for various harmonic numbers (1,3,5,7). DELTA:  $E=1.5 \text{ GeV}$ ;  $I=1 \text{ mA}$ .

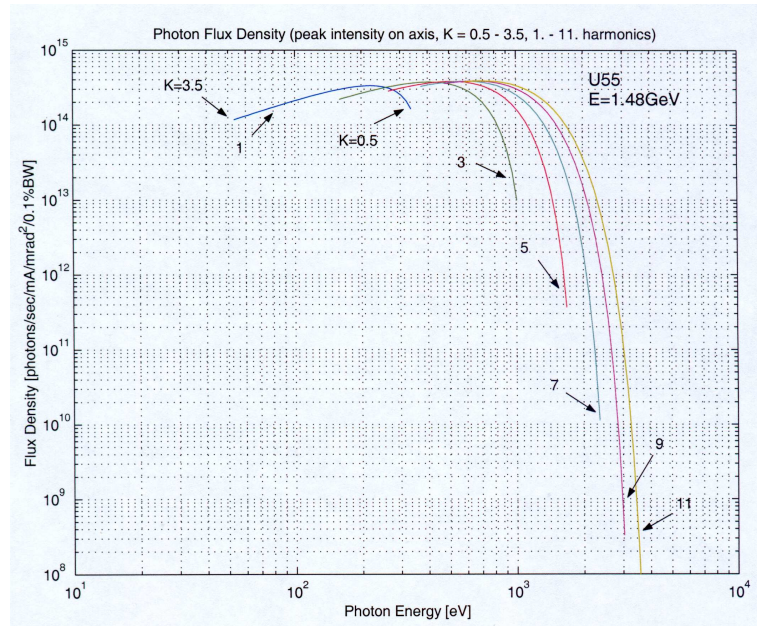


**Fig. 5.10:** Photon flux density (peak intensity on axis) versus photon energy  $E_{ph}$  for various harmonic numbers (1-11) and undulator parameter  $K$  (0.5-3.5). DELTA:  $E=1.48$  GeV;  $I=1$  mA.

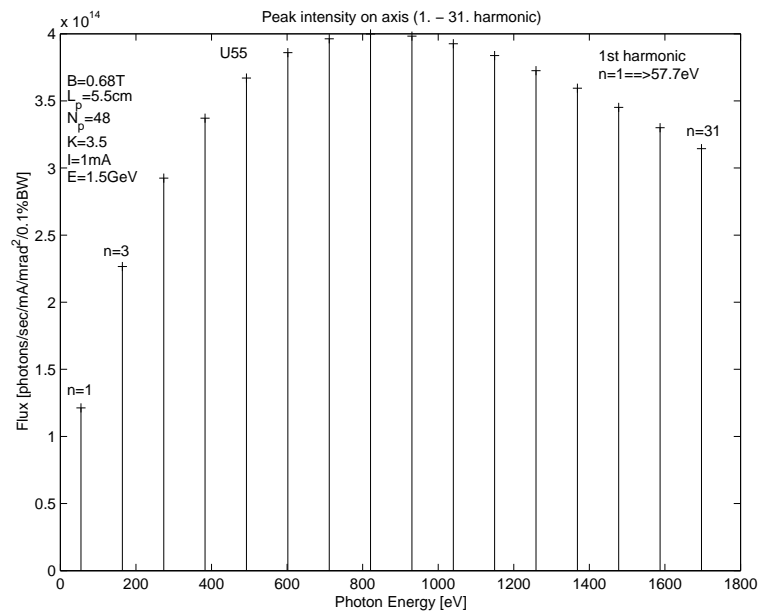


**Fig. 5.11:** Photon flux (peak intensity on axis) versus photon energy (corresponding odd harmonic numbers). DELTA:  $E=1.5$  GeV;  $I=1$  mA.

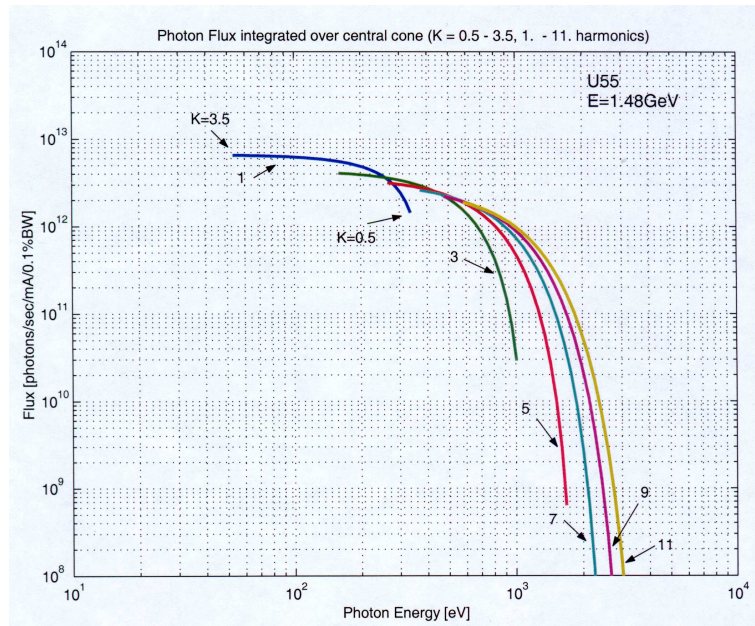


**Fig. 5.12:** Photon flux (integrated over central cone) versus photon energy  $E_{ph}$  for various harmonic numbers (1-11) and undulator parameter  $K$  (0.5-3.5). DELTA:  $E=1.48$  GeV;  $I=1$  mA.

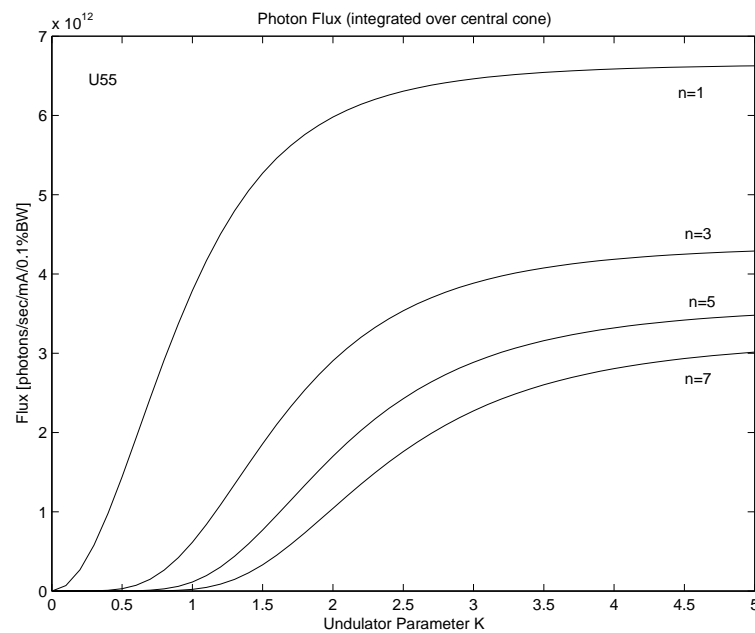


**Fig. 5.13:** Photon flux (integrated over central cone) versus undulator parameter  $K$  for various harmonic numbers (1,3,5,7). DELTA:  $E=1.5$  GeV;  $I=1$  mA.

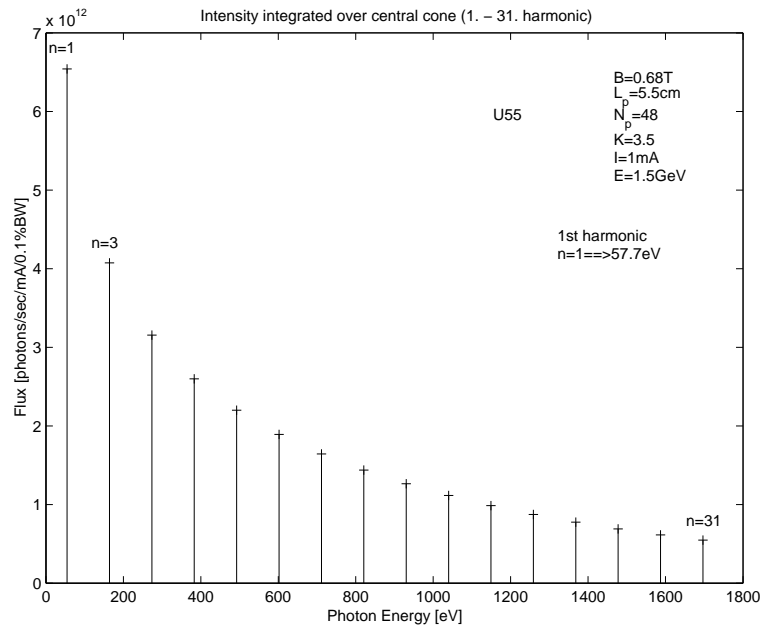


**Fig. 5.14:** Photon flux (integrated over central cone) versus photon energy (corresponding odd harmonic numbers). DELTA:  $E=1.5$  GeV;  $I=1$  mA.

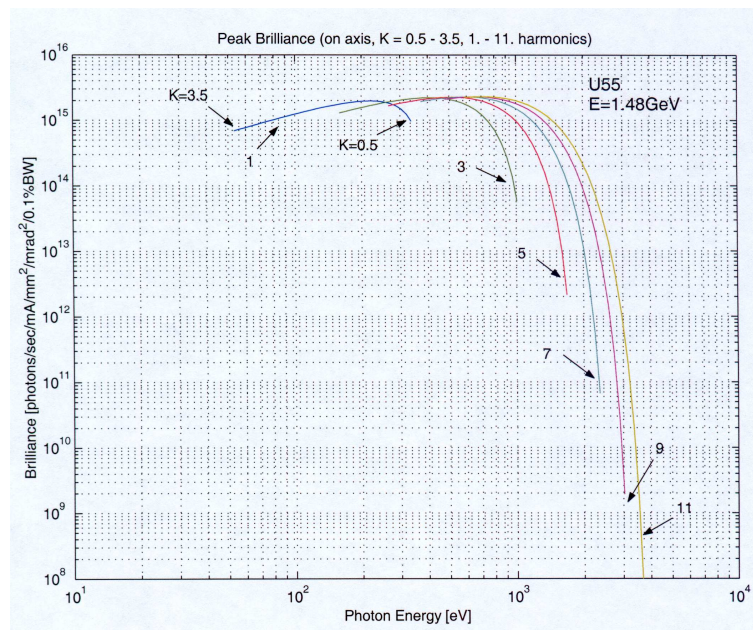


**Fig. 5.15:** Peak Brilliance (on axis) versus photon energy  $E_{ph}$  for various harmonic numbers (1-11) and undulator parameter  $K$  (0.5-3.5). DELTA:  $E=1.48$  GeV;  $I=1$  mA.

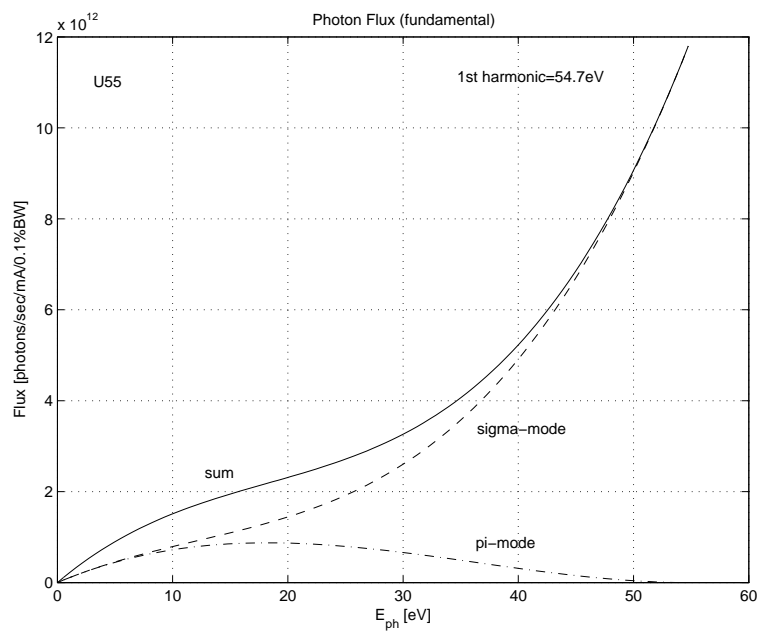


**Fig. 5.16:** Photon flux (fundamental=54.7 eV) versus photon energy  $E_{ph}$ , (horizontal (sigma-mode) and vertical (pi-mode) polarized). DELTA:  $E=1.5$  GeV;  $I=1$  mA.



# A Definitions

**critical (characteristic) photon wavelength:**

$$\lambda_c[\text{\AA}] = \frac{18.64}{E^2[\text{GeV}^2] B[\text{T}]}$$

**critical (characteristic) photon energy:**

$$\epsilon_c[\text{keV}] = 0.665 E^2[\text{GeV}^2] B[\text{T}] = \frac{12.4}{\lambda_c[\text{\AA}]}$$

**undulator respectively wiggler parameter:**

$$K = 0.934 \lambda_u[\text{cm}] B[\text{T}] = \Theta_{\text{hori}}^{\text{max}} \cdot \gamma$$

**spectral photon flux:**

$$[\text{Dim}] = \frac{\text{Photons}}{\text{sec} \times \text{mA} \times 0.1\% \text{BW}}$$

**angular density of spectral photon flux:**

$$[\text{Dim}] = \frac{\text{Photons}}{\text{sec} \times \text{mA} \times (\text{mrad})^2 \times 0.1\% \text{BW}}$$

**brightness / brilliance:**

$$[\text{Dim}] = \frac{\text{Photons}}{\text{sec} \times \text{mA} \times (\text{mrad})^2 \times (\text{mm})^2 \times 0.1\% \text{BW}}$$



## B A numerical approximation of the Bessel Function

For the computation of the synchrotron radiation characteristics frequently one needs the bessel function and its integrals. Whereby  $K_\nu(y)$  represents the modified bessel function of fractional order  $\nu$ , the so called 'Macdonald Function'[29] (see also table 2.1). For this function and its integral no simple, closed analytic expressions exist. Therefore, they must be developed with the help of complex series expansions<sup>1</sup>, or they must be calculated by elaborate numerical integration. A basic representation which can be programmed very simply and sufficiently exact for most applications is given by [31]:

$$K_\nu(y) = h \left[ \frac{1}{2}e^{-y} + \sum_{r=1}^{\infty} e^{-y \cosh(r h)} \cdot \cosh(\nu r h) \right] \quad (\text{B.1})$$

and

$$\int_y^{\infty} K_\nu(y') dy' = h \left[ \frac{1}{2}e^{-y} + \sum_{r=1}^{\infty} e^{-y \cosh(r h)} \cdot \frac{\cosh(\nu r h)}{\cosh(r h)} \right] \quad (\text{B.2})$$

The rapidly converging series expression is terminated when an addend falls below a given 'error barrier'  $\epsilon$  (typical values lie between  $10^{-5} \leq \epsilon \leq 10^{-3}$ ). In computer programs a dynamic adjustment of the sum index  $r$  and the interval width  $h$  under consideration of  $g = \frac{2\pi r}{h}$  in dependence of the error barrier  $\epsilon$  can be implemented. For sufficient accuracy,  $g$  should be chosen adequate large,  $g \gg |\nu|$  and  $|y|$ . For  $\nu = \frac{1}{3}$  or  $\nu = \frac{2}{3}$  one reaches with  $r=20$ ,  $\epsilon \leq 10^{-5}$  and  $h=0.5$  an outstanding consensus for arguments in the mainly used interval from  $y = 100$  to  $y = 10^{-4}$  compared with tabulated bessel function values[30]. Illustration B.1 represents the graphs of the 'universal' wiggler and dipole spectral functions for  $i=1$ . One recognizes that the spectral function of a wiggler for all wavelengths supplies smaller intensities than the appropriate spectral function of a dipole<sup>2</sup> With the help of these general functions all substantial characteristics of the wiggler and dipole radiation can be determined.

---

<sup>1</sup>e.g. hypergeometrical functions[30].

<sup>2</sup>This is to be expected, since the medial local bending radius of a wiggler is larger than that one of an appropriate dipole.

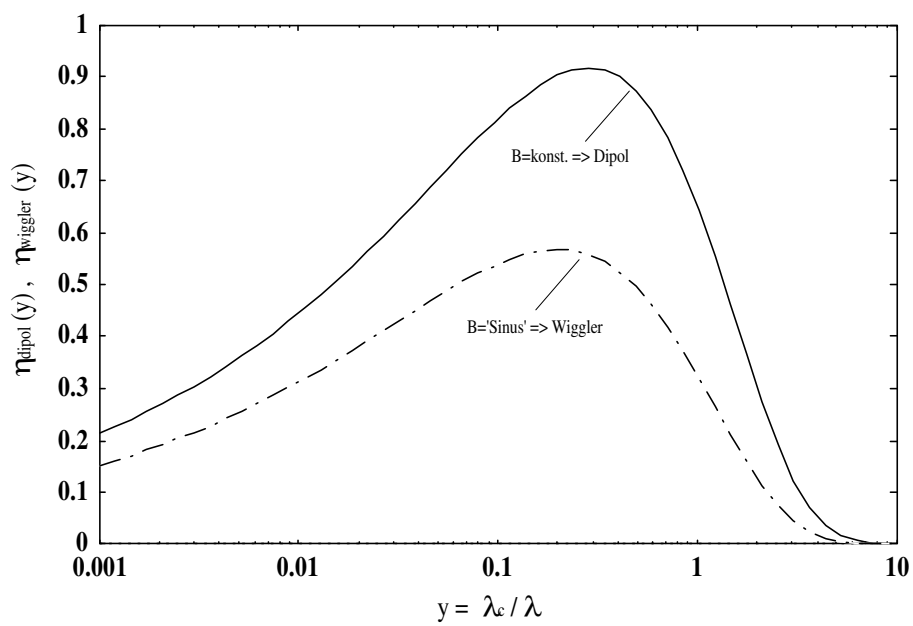


Fig. B.1: Graph of the universal spectral function for wiggler and dipole radiation.

## B.1 Natural opening angle of the synchrotron radiation

Synchrotron radiation occurs in a narrow cone of nominal angular width  $\sim 1/\gamma$ . To provide a more specific measure of this angular width, in terms of the electron and the photon energies, it is convenient to introduce the effective rms half-angle  $\sigma_\psi$  as follows [14], [32]:

$$\sigma_\psi \sqrt{2\pi} = \frac{\frac{dF_D}{d\theta}}{\left. \frac{d^2 F_D}{d\theta d\psi} \right|_{\psi=0}} = \sqrt{\frac{2\pi}{3}} (\gamma y)^{-1} \frac{\int_y^\infty K_{5/3}(y') dy'}{K_{2/3}^2(y/2)} \equiv \frac{1}{\gamma} \cdot C(y) \quad (\text{B.3})$$

The graph for the function  $\sigma_\psi$  is plotted in figure B.2. A good approximation for  $\sigma_\psi$  is given by (with  $\lambda/\lambda_c = 1/y$ ):

$$\sigma_\psi \approx \frac{2}{\gamma \sqrt{2\pi}} \cdot C(y) = 0.408 \frac{C(y) [\text{mrad}]}{E [\text{GeV}]} \quad (\text{B.4})$$

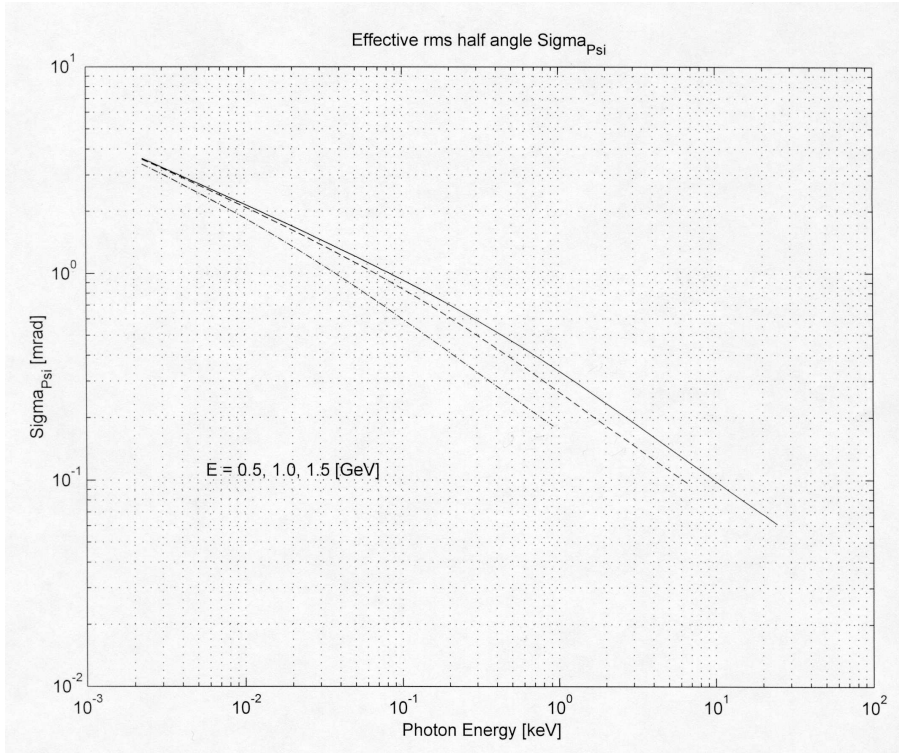


**Fig. B.2:** Effective rms half SR opening angle  $\sigma_\psi$  versus photon energy for various electron energies (0.5 GeV dot dashed line, 1.0 GeV dashed line, 1.5 GeV continuous line).



## C Comparison to other Synchrotron Radiation Sources

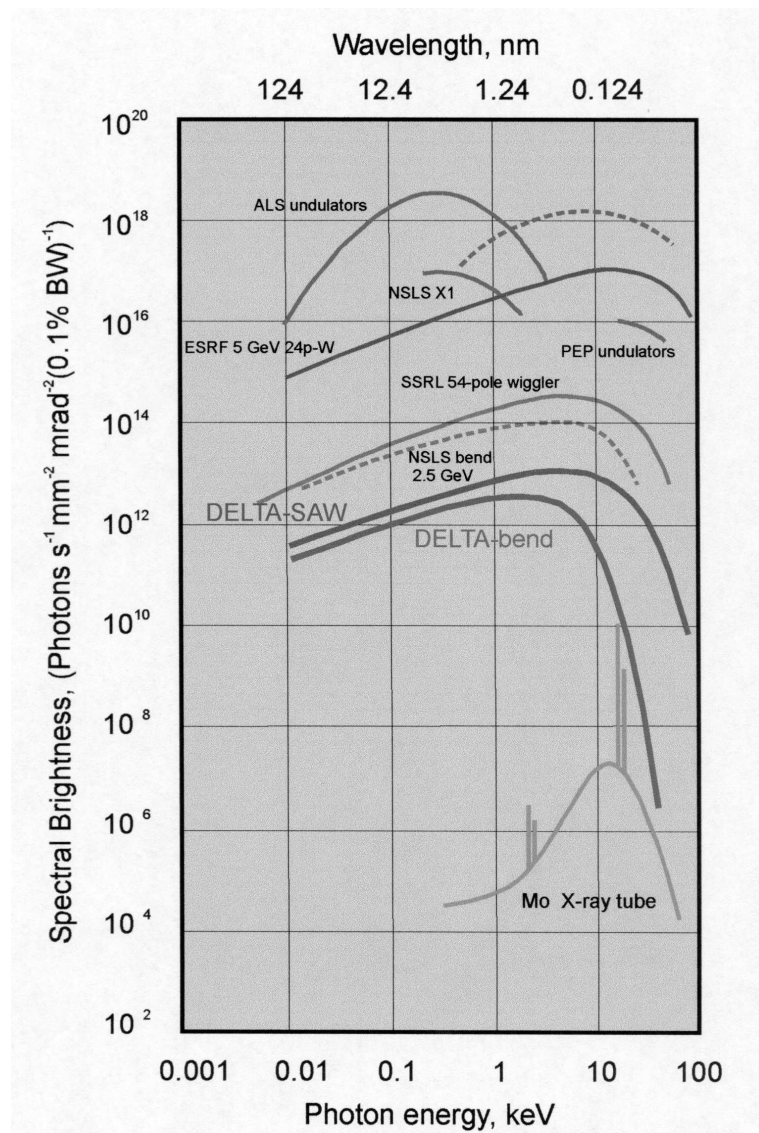
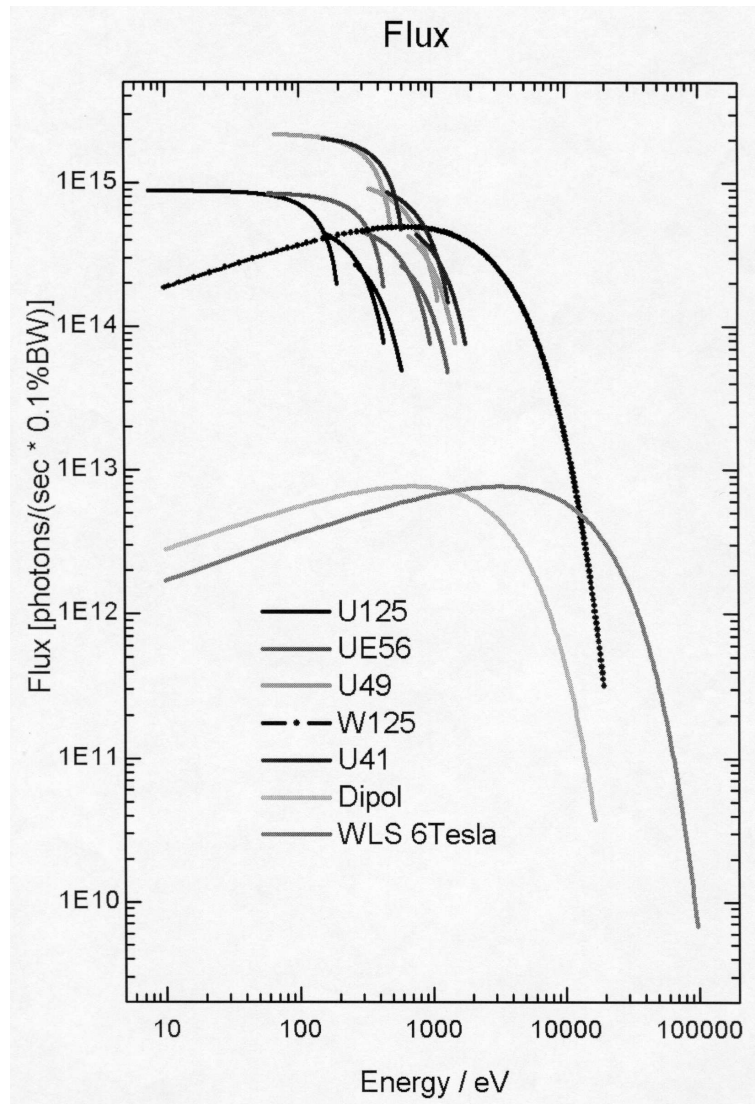
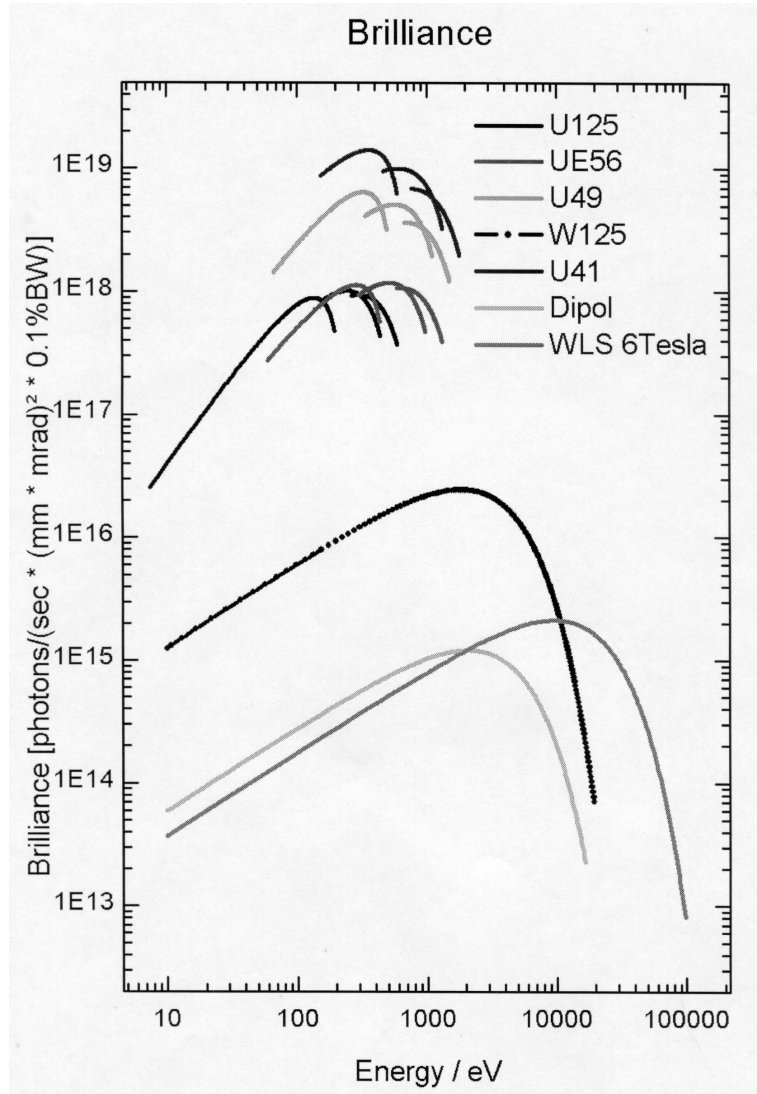


Fig. C.1: DELTA in comparison to other synchrotron radiation sources [33].



**Fig. C.2:** Flux curves of the BESSY insertion devices (@100 mA)  
([http://bessy.de/users\\_info/](http://bessy.de/users_info/)).



**Fig. C.3:** Brilliance curves of the BESSY insertion devices (@100 mA) ([http://bessy.de/users\\_info/](http://bessy.de/users_info/)).



# List of Figures

1.1	<i>Beamlines and magnet lattice of the DELTA facility.</i>	1
1.2	<i>Brilliance of various SR-sources at DELTA (electron beam current: 1 mA, horizontal emittance: 16 nm rad at 1.48 GeV).</i>	3
1.3	<i>Photon flux density of various SR-sources at DELTA (electron beam current: 1 mA, horizontal emittance: 16 nm rad at 1.48 GeV).</i>	4
1.4	<i>Photon flux of various SR-sources at DELTA (electron beam current: 1 mA, horizontal emittance: 16 nm rad at 1.48 GeV).</i>	4
2.1	<i>Coordinate system to describe the motion of charged particles and the angular dependence of the synchrotron radiation properties.</i>	8
2.2	<i>Definitions of the emittance ellipse in the phase space.</i>	14
2.3	<i>Optical functions (betafuncions <math>\beta_{x,y}</math> and dispersion <math>\eta_x</math>) along the orbit position <math>s</math> (DELTA-008 standard optics; SAW off).</i>	15
2.4	<i>Optical functions (betafuncions <math>\beta_{x,y}</math> and dispersion <math>\eta_x</math>) along the orbit position <math>s</math> (DELTA-008 standard optics; SAW on).</i>	15
3.1	<i>DELTA dipole magnet.</i>	19
3.2	<i>Vertical integrated photon flux (number of photons at a given wavelength/energy within a given bandwidth, integrated over all vertical opening angles) for different storage ring energies.</i>	21
3.3	<i>Photon flux in the median plane (<math>\psi = 0</math>) for different storage ring energies.</i>	21
3.4	<i>Spectral distribution of the radiated power (vertical integrated) for different storage ring energies.</i>	22
3.5	<i>Spectral power in the median plane (<math>\psi = 0</math>) for different storage ring energies.</i>	22
3.6	<i>Vertical integrated spectral photon flux distribution of the parallel (sigma) and perpendicular (pi) components of the electric field vector with respect to the orbit plane (@1.5GeV).</i>	23
3.7	<i>Degree of linear and circular polarization as a function of photon energy.</i>	23
3.8	<i>Vertical angular distribution of parallel (sigma) and perpendicular (pi) polarization components (for 10 keV photons).</i>	24
3.9	<i>Linear and circular polarization as a function of the vertical emission angle (for 10 keV photons)</i>	24
3.10	<i>Flux, flux density and brilliance generated by a DELTA bending magnet (here @ ISAS BL-2). DELTA beam current: 1mA</i>	25
4.1	<i>Superconducting Asymmetric Wiggler (SAW).</i>	27
4.2	<i>Vertical magnetic field component along the wiggler axis (full wiggler length).</i>	30

4.3	<i>Vertical magnetic field component along the wiggler axis (one asymmetric period). Comparison of FFT fit of the measured data [8] and the theoretical optimized model [22]. . . . .</i>	31
4.4	<i>Angular deflection and orbit displacement along the wiggler axis (here for measured data). . . . .</i>	31
4.5	<i>Parametric plot of deflection angle vs. magnetic field respectively critical photon energy. . . . .</i>	32
4.6	<i>Magnetic field contributions from the positive and negative magnetic field components. . . . .</i>	32
4.7	<i>Total photon flux versus horizontal deflection angle (here: <math>E_{ph} = 10</math> keV and one wiggler period). . . . .</i>	33
4.8	<i>Photon flux (<math>\sigma</math>- and <math>\pi</math>-mode) and degree of polarization generated by the negative and positive magnetic field components (here: <math>E_{ph} = 10</math> keV and one wiggler period). . . . .</i>	33
4.9	<i>Degree of linear (P) and circular (Tau) polarization in dependence of the horizontal deflection angle (here: <math>E_{ph} = 10</math> keV and one wiggler period). . . . .</i>	34
4.10	<i>Spectral photon flux (vertical integrated) for the center SAW BL-9. Superposition of 5 strong (5.3 T) and 4 weak (-2.1 T) SAW magnetic field components. The DELTA dipole radiation is shown for comparison. . . . .</i>	34
4.11	<i>Analogous to figure 4.10. Here emphasis on the X-ray range of the spectrum. . . . .</i>	35
4.12	<i>Photon flux , flux density and brilliance for the center SAW BL-9. . . . .</i>	35
4.13	<i>Degree of linear (P) and circular (Tau) polarization in dependence of the photon energy for the center SAW BL-9. . . . .</i>	36
4.14	<i>Degree of linear (P) and circular (Tau) polarization for a photon energy of 13.5 keV in dependence of the vertical emission angle (center SAW BL-9). . . . .</i>	36
4.15	<i>Vertical angular distribution of parallel (sigma) and perpendicular (pi) polarization components (photon flux for 1 keV photons) (center SAW BL-9). . . . .</i>	37
4.16	<i>Vertical angular distribution of parallel (sigma) and perpendicular (pi) polarization components (photon flux for 13.5 keV photons) (center SAW BL-9). . . . .</i>	37
4.17	<i>Spectral power in the median plane (<math>\psi = 0</math>) (center SAW BL-9). . . . .</i>	38
4.18	<i>Spectral distribution of the radiated power (vertical integrated) (center SAW BL-9). . . . .</i>	38
5.1	<i>Electromagnetic undulator U250. . . . .</i>	39
5.2	<i>Photon flux (peak intensity on axis) versus undulator parameter K for various harmonic numbers (1,3,5,7). DELTA: (<math>E=1.5</math>GeV; <math>I=1</math>mA). . . . .</i>	40
5.3	<i>Photon flux (integrated over central cone) versus undulator parameter K for various harmonic numbers (1,3,5,7). DELTA: (<math>E=1.5</math>GeV; <math>I=1</math>mA). . . . .</i>	41
5.4	<i>Photon flux (peak intensity on axis) versus photon energy (corresponding odd harmonic numbers 1-31). DELTA: (<math>E=1.5</math>GeV; <math>I=1</math>mA). . . . .</i>	41
5.5	<i>Photon flux (integrated over central cone) versus photon energy (corresponding odd harmonic numbers 1-31). DELTA: (<math>E=1.5</math>GeV; <math>I=1</math>mA). . . . .</i>	42
5.6	<i>Photon flux (fundamental=26.3eV) versus photon energy <math>E_{ph}</math>, (horizontal (sigma-mode) and vertical (pi-mode) polarized). DELTA: (<math>E=1.5</math>GeV; <math>I=1</math>mA). . . . .</i>	42
5.7	<i>Undulator parameter K versus photon energy <math>E_{ph}</math> for various harmonic numbers (1,3,5,7), DELTA: (<math>E=1.5</math>GeV; <math>I=1</math>mA). . . . .</i>	43

5.8	<i>Permanent magnets undulator U55.</i>	44
5.9	<i>Photon flux (peak intensity on axis) versus undulator parameter <math>K</math> for various harmonic numbers (1,3,5,7). DELTA: <math>E=1.5</math> GeV; <math>I=1</math> mA.</i>	45
5.10	<i>Photon flux density (peak intensity on axis) versus photon energy <math>E_{ph}</math> for various harmonic numbers (1-11) and undulator parameter <math>K</math> (0.5-3.5). DELTA: <math>E=1.48</math> GeV; <math>I=1</math> mA.</i>	46
5.11	<i>Photon flux (peak intensity on axis) versus photon energy (corresponding odd harmonic numbers). DELTA: <math>E=1.5</math> GeV; <math>I=1</math> mA.</i>	46
5.12	<i>Photon flux (integrated over central cone) versus photon energy <math>E_{ph}</math> for various harmonic numbers (1-11) and undulator parameter <math>K</math> (0.5-3.5). DELTA: <math>E=1.48</math> GeV; <math>I=1</math> mA.</i>	47
5.13	<i>Photon flux (integrated over central cone) versus undulator parameter <math>K</math> for various harmonic numbers (1,3,5,7). DELTA: <math>E=1.5</math> GeV; <math>I=1</math> mA.</i>	47
5.14	<i>Photon flux (integrated over central cone) versus photon energy (corresponding odd harmonic numbers). DELTA: <math>E=1.5</math> GeV; <math>I=1</math> mA.</i>	48
5.15	<i>Peak Brilliance (on axis) versus photon energy <math>E_{ph}</math> for various harmonic numbers (1-11) and undulator parameter <math>K</math> (0.5-3.5). DELTA: <math>E=1.48</math> GeV; <math>I=1</math> mA.</i>	48
5.16	<i>Photon flux (fundamental=<math>54.7</math> eV) versus photon energy <math>E_{ph}</math>, (horizontal (sigma-mode) and vertical (pi-mode) polarized). DELTA: <math>E=1.5</math> GeV; <math>I=1</math> mA.</i>	49
B.1	<i>Graph of the universal spectral function for wiggler and dipole radiation.</i>	54
B.2	<i>Effective rms half SR opening angle <math>\sigma_\psi</math> versus photon energy for various electron energies (0.5 GeV dot dashed line, 1.0 GeV dashed line, 1.5 GeV continuous line).</i>	55
C.1	<i>DELTA in comparison to other synchrotron radiation sources [33].</i>	57
C.2	<i>Flux curves of the BESSY insertion devices (@100 mA) (<a href="http://bessy.de/users_info/">http://bessy.de/users_info/</a>).</i>	58
C.3	<i>Brilliance curves of the BESSY insertion devices (@100 mA) (<a href="http://bessy.de/users_info/">http://bessy.de/users_info/</a>).</i>	59



# List of Tables

1.1	<i>Important machine and operating parameters (Status 1/2005).</i>	5
2.1	<i>Nomenclature of the most important physical constants, abbreviations and substitutions.</i>	12
2.2	<i>Twiss parameter (DELTA-008 optics) at various beamlines (BL-0 ... BL-12).</i>	16
2.3	<i>Beam size and divergence at various beamlines (BL-0 ... BL-12).</i>	16
2.4	<i>Data for the pulsed time structure of the synchrotron radiation at DELTA.</i>	17
3.1	<i>Bending magnet data.</i>	20
3.2	<i>Characteristic DELTA dipole SR data at different storage ring energies.</i>	20
4.1	<i>Main wiggler parameter.</i>	28
4.2	<i>Peak field at various coil excitations for the symmetric and asymmetric SAW mode.</i>	29
5.1	<i>Main data of the electromagnetic FEL undulator magnet U-250 (@1.5GeV).</i>	40
5.2	<i>Parameters of the U-55 hybrid undulator.</i>	45



## Bibliography

- [1] T. Weis, U. Berges, J. Friedl, P. Hartmann, R. Heine, H. Huck, J. Kettler, O. Kopitzki, D. Schirmer, G. Schmidt, and K. Wille. Status of the 1.5 GeV Synchrotron Light Source DELTA and related Accelerator Physics Activities. In *RuPAC, Novosibirsk*, 2006.
- [2] U. Berges et al. Status of the Light Source DELTA. In *Proc. Synchr. Rad. Instr., Korea*, 2006.
- [3] D. Schirmer, U. Berges, J. Friedl, A. Gasper, M. Grewe, P. Hartmann, R. Heine, H. Huck, G. Schmidt, C. Sternemann, H. Tolan, T. Weis, C. Westphal, K. Wille, and N. Zabrala. Status of the Synchrotron Light Source DELTA. In *EPAC, Lucerne, Switzerland*, 2004.
- [4] G. Schmidt, U. Berges, K. Dunkel, J. Friedl, A. Gasper, M. Grewe, P. Hartmann, R. Heine, E. Kasel, B. Keil, D. Schirmer, T. Weis, K. Wille, and D. Zimoch. Status of the Synchrotron Light Source DELTA. In *EPAC, Paris, France*, 2002.
- [5] C. Sternemann. private communication, 2004.
- [6] Alex von Bohlen. Report 2006, Second DELTA User-Metting. Technical report, DELTA, 29. Nov. 2006.
- [7] Alex von Bohlen. Report 2005, First DELTA User-Metting. Technical report, DELTA, 30. Nov. 2005.
- [8] ACCEL Instruments GmbH, D-51429 Bergisch Gladbach, Germany, 1998, 1999.
- [9] U. Berges. private communication, 2007.
- [10] G. Schott. *Electromagnetic Radiation*. Cambridge Univ. Press, 1912.
- [11] J. Schwinger. On the classical radiation of accelerated electrons. *Phys. Rev.* 75,12, pages 1912–1925, 1949.
- [12] A. A. Sokolov and I. M. Ternov. *Synchrotron Radiation*. Pergamon, 1968.
- [13] J. D. Jackson. *Klassische Elektrodynamik*. de Gruyter, Berlin, New York, second edition, 1982.
- [14] K. J. Kim. Characteristics of Synchrotron Radiation. *LBL, AIP*, pages p. 565–632, 1989.
- [15] A. Ropert. *High Brilliance Lattices and the effects of Insertion Devices*. ESRF (Grenoble), 1989.

- [16] D. Schirmer and K. Wille. Delta Optics. In *IEEE Particle Accelerator Conference 1991*, volume 5, pages 2859–2861, San Francisco, California, May 6-9 1991.
- [17] A. Geisler, M. Ridder, and T. Schmidt. Int. rep. 94-8. Technical report, DELTA, 1994.
- [18] A. Geisler. private communication, 1998.
- [19] D. Schirmer, M. Grewe, E. Kasel, B. Keil, K. Wille, and D. Zimoch. First Experience with the Superconducting Asymmetric Wiggler of the DELTA Facility. In *EPAC, Wien, Austria*, 2000.
- [20] T. Roy. Optimierung des DELTA-Speicherring für den Betrieb des neuen supraleitenden Wigglermagneten. Master's thesis, University of Dortmund, 1999.
- [21] M. Negrazus and A. Peters. SAW - A Superconducting Asymmetric Multipole Wiggler at the DELTA Storage Ring. In *EPAC, Barcelona, Spain*, 1996.
- [22] D. Schirmer. Design Study of a Superconducting Asymmetric Multipole-Wiggler for the 1.5 GeV Storage Ring DELTA for Variably Polarized X-Ray Synchrotron Radiation. In *XV<sup>th</sup> International Conference on High Energy Accelerators, HEACC'92*, Hamburg, Germany, July 1992.
- [23] D. Schirmer. PhD thesis, University of Dortmund, Germany, 1994.
- [24] DELTA-FEL-Gruppe. The pulsed wire method, an alternative magnetic field measurement technique. Technical report, DELTA, Int. Rep. 95-8, 1995.
- [25] Thomas Schmidt. *Aufbau des FEL Experiments FELICITA I im sichtbaren und ultravioletten Spektralbereich am Speicherring DELTA*. PhD thesis, University of Dortmund, 1997.
- [26] A. Hoffmann. Theory of synchrotron radiation. *SSRL*, (ACD-Note 38), Sept. 1986.
- [27] K. Halbach. In *Proc. SPIE Intern. Conf. on Insertion Devices for Synchrotron Sources*, SPIE, pages 133–139, Stanford, CA, 1985.
- [28] K. Wille. *Physik der Teilchenbeschleuniger und Synchrotronstrahlungsquellen*. Teubner Studienbücher, Physik, 1992.
- [29] L. D. Landau and E. M. Lifschitz. *Klassische Feldtheorie*, volume 2. Akademie Verlag, Berlin, 1984. 11. Auflage.
- [30] M. Abramowitz and I. A. Stegun. *Handbook of Mathematical Functions*. Dover Publ. (New York), Ninth Printing, 1970.
- [31] V. O. Kostroun. Simple numerical evaluation of modified bessel functions  $K_{\nu}(x)$  of fractional order and the integral  $\int_x^{\infty} K_{\nu}(\eta)d\eta$ . *NIM*, 172, pages 371–374, 1980.
- [32] K. J. Kim. Brightness and Coherence of Synchrotron Radiation and High Gain Free Electron Lasers. In *Proc. of the VII Nat. Conf. on Synchrotron Radiation(SR86)*, Novosibirsk, USSR, 1986.
- [33] Alex von Bohlen. private communication, 2005.